Soft Matter

Induced Stabilization of Columnar Phases in Binary Mixtures of Discotic Liquid Crystals

Journal:	*Soft Matter*
Manuscript ID	SM-ART-08-2015-001959.R2
Article Type:	Paper
Date Submitted by the Author:	08-Nov-2015
Complete List of Authors:	Cienega-Cacerez, Octavio; Universidad Autónoma Metropolitana-Iztapalapa, Physics García-Alcántara, Consuelo; Universidad Nacional Autónoma de México, Campus Juriquilla, Physics Moreno-Razo, José; Universidad Autónoma Metropolitana-Iztapalapa, Physics Díaz-Herrera, Enrique; Universidad Autónoma Metropolitana-Iztapalapa, Physics Sambriski, Edward; Delaware Valley University, Chemistry

Journal Name

ARTICLE TYPE

Cite this: DOI: 10.1039/xxxxxxxxxx

Induced Stabilization of Columnar Phases in Binary Mixtures of Discotic Liquid Crystals

Octavio Cienega-Cacerez[a], Consuelo García-Alcántara[a,b], José Antonio Moreno-Razo[a], Enrique Díaz-Herrera[a], and Edward John Sambriski*[c]

Received Date
Accepted Date

DOI: 10.1039/xxxxxxxxxx

www.rsc.org/journalname

Three discotic liquid-crystalline binary mixtures, characterized by their extent of bidispersity in molecular thickness, were investigated with Molecular Dynamics simulations. Each equimolar mixture contained A-type (*thin*) and B-type (*thick*) discogens. The temperature-dependence of the orientational order parameter reveals that A-type fluid samples tend to produce ordered phases more readily, with the (hexagonal) columnar phase being the most structured variant. Moderately and strongly bidisperse mixtures produce globally-segregated samples for temperatures corresponding to ordered phases; the weakly bidisperse mixture displays microheterogeneities. Ordered phases in the B-type fluid are induced partially by the presence of the A-type fluid. In the moderately bidisperse mixture, order is induced through orientational frustration: a mixed *prenematic*-like phase precedes global segregation to yield nematic and columnar mesophases upon further cooling. In the strongly bidisperse mixture, order is induced less efficiently through a *paranematic*-like mechanism: a highly-ordered A-type fluid imparts order to B-type discogens found at the interface of a fully-segregated sample. This ordering effect permeates into the disordered B-type domain until nematic and columnar phases emerge upon further cooling. At sufficiently low temperatures, all samples investigated exhibit the (hexagonal) columnar mesophase.

1 Introduction

Discotic liquid crystals (DLCs) consist of anisotropic molecules (i.e., discogens) with a polycyclic (typically aromatic) core, yielding a flat- and rigid-like template[1,2]. Like their calamitic (rod-like) counterparts, DLCs have the ability to form mesophases intermediate between solid and liquid states of matter, with varying extents of orientational and translational order[1,3,4]. Although DLCs exhibit a variety of orientational phase transitions, those commonly observed are isotropic, nematic, and columnar phases[1,5–17]. The columnar phase is of particular interest due to its ferroelectric behavior[18,19], photoconduction[20–26], and electrical conduction[24,27–29]. Charge transport is quasi-one-dimensional, facilitated primarily along the columnar axis when peripheral groups attached to the core provide insulation from neighboring columns[1,30,31]. These properties have been exploited to produce DLC-based devices[32], including photovoltaic modules, light-emitting diodes, field effect transistors, memory elements, and sensors[28,30,33–37]. The columnar phase also possesses intrinsic uniaxial negative birefringence: the refractive index in the core plane is higher than along the columnar axis. This feature has been applied in compensation films with a tilted optical axis in liquid crystal displays, either to expand the viewing angle or to enhance the contrast ratio[38–42].

The columnar phase forms when discogens stack on top of one another to produce a "column" of fluid, aligning their molecular axes (being normal to the plane of the core) along a common axis. The stacking of polyaromatic cores is prompted by π-π interactions, which stabilize the mesophase and shape conduits for charge transport[43–48]. The resulting columns can pack into a two-dimensional array of helical, hexagonal, lamellar, oblique, rectangular, or tilted geometries[1,5–17,30,49]. The face-to-face distance of molecules in the columnar phase is about 0.3 nm, whereas the intercolumnar separation is approximately 2-4 nm, depending on the nature and distribution of peripheral groups around the disco-

[a] *Departamento de Física*
Universidad Autónoma Metropolitana-Iztapalapa
Avenida San Rafael Atlixco No. 186
Colonia Vicentina, Delegación Iztapalapa
México, D.F. 09340 México
[b] *Unidad Multidisciplinaria de Docencia e Investigación-Juriquilla*
Facultad de Ciencias
Universidad Nacional Autónoma de México, Campus Juriquilla
Boulevard Juriquilla 3001
Juriquilla, Querétaro 76230 México
[c] *Department of Chemistry*
Delaware Valley University
700 East Butler Avenue
Doylestown, Pennsylvania 18901 USA
Tel: +1 215 4894785; Fax: +1 215 4894960
E-mail: Edward.Sambriski@delval.edu

gen core [1]. Columnar interspacing and geometry is tunable with functional groups (e.g., alkyl-, ester- or ether-based chains) covalently bonded to and extending from the core periphery.

Because many DLC-based applications require the columnar phase, chemical systems are chosen for their ability to yield the mesophase at convenient working conditions [50]. One way of extending the stability and versatility of these materials is to formulate mixtures. Given that some properties of mixtures depend on the "mixed" or "microsegregated" state, a complete description requires the conditions stabilizing the homogeneity of components or leading to microphase separation. Moreover, the properties of mixtures can differ substantially and uniquely from those of the corresponding components: predicting the behavior of mixtures is not a simple matter of interpolating properties. For instance, consider these two examples involving liquid-crystalline behavior: (*a*) a substance with no mesogenic character when combined with another non-mesogenic compound yields a mixture capable of producing liquid-crystalline mesophases [51,52], and (*b*) a non-covalent intermolecular interaction (known as the *complementary polytopic interaction* or CPI) emerges only in a mixture to produce a stable mesophase [50,53–60], thus contesting rationalizations based on dipolar and quadrupolar contributions [53,57].

DLCs are characterized by rich phase behavior [6,61–70], including biphasic and reentrant phase transitions [65,71–82]. The phase behavior of DLC mixtures is even more complex because fractionation (i.e., demixing) of components is coupled with orientational transitions [83]. Moreover, the presence of another component can prompt and stabilize a mesophase over a wider temperature range [51,84,85], or cause another component that has segregated completely from a mixture (thus yielding a type-pure domain) to behave differently from the corresponding pure liquid [86]. In addition to describing intercolumnar arrangements and intra (or intra-alternating) columnar separation, it is also of interest to consider liquid-crystalline structures that result from local-scale interfacial effects [45,47,87–89], thin films [90–100], substrates [101–106], or dopants [25,28,107–123].

Experiments have showcased the versatility possible with DLC mixtures. Compounds that behave with a CPI paradigm [50,53–60], in which disc types alternate by "fastening" on top of one another, can yield a columnar phase with enhanced electrical conduction and a wider temperature range of stability [56,60,124,125]. These features are critical in rendering useful, DLC-based devices [49,126,127]. Another route has involved mixing two discogens with different electronic properties [128] to yield a columnar phase in which donor and acceptor molecules alternate along a columnar axis. This arrangement has led to enhanced charge-carrier mobilities in comparison to single-component (i.e., pure) systems. A number of studies have outlined design principles for optimizing the integrity of the columnar phase [31,50,56,129] and have highlighted features that improve the performance. For instance, it has been found that charge-carrier mobility is increased with long-range alloy band structure [56,129]. These observations provide a strong basis for the continued study of DLC mixtures as a means to expand their technological use and industrial processability.

Despite the importance of extending the application range of DLCs, their mixtures have been treated to a limited degree in computational and theoretical fronts. The role of attractive interactions in reproducing phase behavior data with density functional theory (DFT) for pure discotic molecules was first addressed by Coussaert and Baus [130]. Mixed-geometry mixtures of a DLCs (i.e., disc-like bodies with rod-like [calamitic], spherical, or other geometrical bodies) have been studied with hard-body models, relevant to lyotropic (colloidal) liquid-crystal mixtures. Disc-like particle/sphere and disc-like particle/polymer mixtures were addressed by de las Heras and Schmidt using DFT [131]. Galindo et al. treated a mixture of rod-like and disc-like particles with Monte Carlo (MC) simulations, focusing on the demixing behavior as the density is increased [132]. The same mixture was studied with MC simulations, Parsons-Lee theory, and experiment from which detailed phase behavior was obtained [133]. Gamez et al. studied disc-like/spherical particle mixtures using Parsons-Lee theory, the results of which were compared to MC simulations [134]. Several aspects of this mixture were observed, such as the stability against demixing up to very high packing fractions and crowding effects. The phase behavior of several of these mixed-geometry mixtures of DLCs have also been treated experimentally [135–137].

Computational and theoretical studies on mixtures involving disc-like particles exclusively are less common. Phillips and Schmidt used DFT to elucidate the demixing in a binary mixture of platelets with different radial ratios [138]. Lekkerkerker and co-workers [139] treated the multiphase coexistence in suspensions of hard (disc-like) platelets using osmotic equilibrium theory. Their approach reproduced semi-quantitatively the experimental studies of Nakato and co-workers [140], which provide evidence on the influence depletion attractive forces have on the coexistence of isostructural ordered phases. Golmohammadi and Rey used a Maier-Saupe model to study a binary mixture of discotics [141,142], where nematic ordering can be tuned by molecular interaction parameters and molar mass disparities. Cinacchi and Tani studied with MC simulations pure systems and non-equimolar mixtures of disc-like particles [143]. The authors used an *S*-function Corner potential to investigate the combined effects of shape and concentration in the mixtures on the liquid structure. Chemically-induced liquid-crystalline phases with quadrupolar Gay-Berne discs were treated by Bates and Luckhurst [144,145]. More recently, Zannoni and co-workers investigated the interface of a donor-acceptor DLC couple with a united-atom Molecular Dynamics (MD) simulation and compared those results with experiment [146]. The authors found that a column mismatch at the donor-acceptor interface improves the performance of a DLC-based solar cell.

To our knowledge, an MD study on the bidispersity of DLC mixtures (varied systematically) is still lacking in the literature. Of particular interest is the influence that such mixtures could have on expanding the range of material properties in technological applications. The aim of the present work is to model demixing and orientational transitions in *thermotropic* DLC binary mixtures. Attention is given in this work to how orientational phase transitions are affected by a dispersity in disc aspect ratios, specialized to the case of thickness bidispersity. Although thickness bidispersity is not commonly treated in computational studies, it is an important variant with application to molecular cores involved in CPI-based systems. This approach represents an alternative

to the chemical induction of columnar phases by a quadrupolar effect[144,145]. Our study focuses on the structural behavior of liquid-crystalline mesophases and demixing transitions. Some aspects treated in this work were previously addressed for calamitic LC mixtures[86] via MD simulations. The present work offers an extension to discotic mixtures. Recently, we reported our findings for the phase behavior, fluid structure, and diffusivity of a discogen bulk sample, using a Gay-Berne parameterization for a triphenylene-like core[147]: this parameterization is implemented as a disc type for one of the mixtures in this study.

Binary mixtures of discotic mesogens are treated in this work by varying the dispersity in molecular aspect ratios through a Gay-Berne model (in which the semi-major axis of the discogen is held constant). The content is organized in the following manner: the model, simulation details, and background information for system characterization are presented in Section 2. Simulation data and a discussion of results are presented in Section 3; the bidispersity of each system is first explored in detail and trends are then outlined collectively. Finally, a summary of our findings and an outlook for this study is presented in Section 4.

2 Model Description and Simulations

2.1 Generalized Gay-Berne Model

Binary mixtures considered in this work consist of A-type (*thin*) and B-type (*thick*) discogens. When referring to type-resolved contributions in a mixture, subscripted indices ab will imply $ab \in \{\mathrm{A},\mathrm{B}\}$, so that all possible self- and cross-terms are taken into account (i.e., AA, BB, AB, and BA). Note that for some properties, AB $\neq$ BA. When describing a pure (one-component) liquid or a specific self-term in the mixture, a double-indexed designation aa is used (i.e., implying AA- and BB-terms only). Although redundant, the aa designation is introduced for consistency and to avoid using another scheme for pure or specific type-resolved terms (i.e., properties denoted with a putative single index a).

Discogens in the system are characterized by a thickness $\sigma_{\mathrm{f},aa}$ and a diameter $\sigma_{0,aa}$. A binary mixture or a pure liquid is characterized by a total of N discogens. The concentration of each type of discogen in a mixture is specified by a number (molar) fraction x_{aa}, such that $x_{\mathrm{AA}} + x_{\mathrm{BB}} = 1$. Thus, the number of A-type discogens in a binary mixture is $N_{\mathrm{AA}} = x_{\mathrm{AA}}N$ and the total number of discogens in the mixture is given by $N = N_{\mathrm{AA}} + N_{\mathrm{BB}}$.

Discogens interact through a generalization[148] of the standard Gay-Berne (GB) potential[149], extended to binary mixtures as

$$U_{ab}\left(\mathbf{r}_{ij},\hat{\mathbf{u}}_i,\hat{\mathbf{u}}_j\right) = 4\,\varepsilon_{ab}\left(\hat{\mathbf{r}}_{ij},\hat{\mathbf{u}}_i,\hat{\mathbf{u}}_j\right)\left(\Xi_{ij}^{-12} - \Xi_{ij}^{-6}\right), \qquad (1)$$

where all self- and cross-terms (i.e., ab) for molecular interactions are taken into account, $\hat{\mathbf{r}}_{ij} = \mathbf{r}_{ij}/r_{ij}$ is the unit vector along the center-to-center vector $\mathbf{r}_{ij}$ between discogens (with r_{ij} being the norm of $\mathbf{r}_{ij}$, i.e., $r_{ij} = |\mathbf{r}_{ij}|$), and $\hat{\mathbf{u}}_i$ as well as $\hat{\mathbf{u}}_j$ are unit vectors along the principal axis (i.e., molecular director) of discogens i and j, respectively. The GB potential captures pairwise interactions between anisotropic, coarse-grained molecules. The relevant geometry for a discotic molecule in the context of the Gay-Berne model is that of an oblate ellipsoid. Because the GB potential includes repulsive *and* attractive contributions, it is possible to study temperature-dependent effects in the system, e.g., thermotropic transitions.

Given the GB potential, it is appropriate to define the length scale for Eq. (1) in the case of discogens as

$$\Xi_{ij} = \frac{r_{ij} - \sigma_{ab}\left(\hat{\mathbf{r}}_{ij},\hat{\mathbf{u}}_i,\hat{\mathbf{u}}_j\right) + \sigma_{\mathrm{f},ab}}{\sigma_{\mathrm{f},ab}}, \qquad (2)$$

where

$$\sigma_{\mathrm{f},ab} = \frac{\sigma_{\mathrm{f},aa} + \sigma_{\mathrm{f},bb}}{2}. \qquad (3)$$

The manner in which Eq. (2) defines Ξ_{ij} avoids the unphysical effects previously described by Bates and Luckhurst[150]. To define molecular anisotropies in the binary mixture, a function is introduced for convenience[147],

$$\Gamma(\omega_1,\omega_2) = 1 - \omega_2\left[\frac{{\omega_1}^2 {c_i}^2 + {c_j}^2/{\omega_1}^2 - 2\omega_2 c_i c_j c_{ij}}{1 - {\omega_2}^2 {c_{ij}}^2}\right], \qquad (4)$$

where $c_i \equiv \hat{\mathbf{u}}_i \cdot \hat{\mathbf{r}}_{ij}$, $c_j \equiv \hat{\mathbf{u}}_j \cdot \hat{\mathbf{r}}_{ij}$, and $c_{ij} \equiv \hat{\mathbf{u}}_i \cdot \hat{\mathbf{u}}_j$. The generalized parameters ω_1 and ω_2 are defined subsequently in the model to account for anisotropies in length and energy scales [refer to Eq. (5) and Eq. (14), respectively].

To account for the anisotropy in molecular length scales, the contact distance between discogens i and j is expressed as

$$\sigma_{ab}(\hat{\mathbf{r}}_{ij},\hat{\mathbf{u}}_i,\hat{\mathbf{u}}_j) = \sigma_{0,ab}\left[\Gamma(\alpha_{ab},\chi_{ab})\right]^{-1/2}, \qquad (5)$$

with

$$\sigma_{0,ab} = \frac{\sigma_{0,aa} + \sigma_{0,bb}}{2}. \qquad (6)$$

Note specifically that

$$\sigma_{0,\mathrm{AB}} = \sigma_{0,\mathrm{BA}} = \frac{\sigma_{0,\mathrm{AA}} + \sigma_{0,\mathrm{BB}}}{2} \qquad (7)$$

obeys the Lorentz-Berthelot mixing rule for the core length scale of the two discogen types. The χ_{ab} are generalized molecular anisotropy parameters[148] (with respect to single-component contributions[147,150]), defined as

$$\chi_{ab} = \left[\frac{({\kappa_{aa}}^2 - 1)({\kappa_{bb}}^2 - 1)}{({\kappa_{ab}}^2 + 1)({\kappa_{ba}}^2 + 1)}\right]^{1/2}, \qquad (8)$$

where molecular aspect (width-to-length) ratios are given by

$$\kappa_{ab} = \frac{\sigma_{\mathrm{f},aa}}{\sigma_{0,bb}}, \qquad (9)$$

and the two non-equivalent tee configurations in the binary mixture are distinguished by the α_{ab} parameters, defined as

$${\alpha_{ab}}^2 = \left(\frac{\sigma_{0,aa}}{\sigma_{0,bb}}\right)^2\left[\frac{({\kappa_{aa}}^2 - 1)({\kappa_{ba}}^2 + 1)}{({\kappa_{bb}}^2 - 1)({\kappa_{ab}}^2 + 1)}\right]^{1/2}. \qquad (10)$$

In certain cases (e.g., ellipsoid-sphere mixtures, or prolate-oblate mixtures), χ_{ab} and α_{ab} become imaginary or undefined (due to division by zero). However, in effect only the factors ${\alpha_{ab}}^{\pm 2}\chi_{ab}$ and ${\chi_{ab}}^2$ enter in the definition of $\Gamma(\alpha_{ab},\chi_{ab})$ and the technical issues associated with imaginary roots or undefined model parameters

are circumvented[148].

The intermolecular interaction strength depends on the relative orientation of discogens and takes the form

$$\varepsilon_{ab}(\hat{\mathbf{r}}_{ij},\hat{\mathbf{u}}_i,\hat{\mathbf{u}}_j)=\varepsilon_{0,ab}\left[\varepsilon_{1,ab}(\hat{\mathbf{u}}_i,\hat{\mathbf{u}}_j)\right]^{\nu}\left[\varepsilon_{2,ab}(\hat{\mathbf{r}}_{ij},\hat{\mathbf{u}}_i,\hat{\mathbf{u}}_j)\right]^{\mu}, \quad (11)$$

where $\varepsilon_{0,ab}$ is an energy scale for the interaction well depth when two discogens (one being a-type, the other being b-type) are orthogonal to one another (i.e., cross configuration) and to the center-to-center intermolecular vector (i.e., $\hat{\mathbf{u}}_i\cdot\hat{\mathbf{u}}_j=\hat{\mathbf{u}}_i\cdot\hat{\mathbf{r}}_{ij}=\hat{\mathbf{u}}_j\cdot\hat{\mathbf{r}}_{ij}=0$). The Lorentz-Berthelot mixing rule applies for $\varepsilon_{0,ab}$ in the binary mixture, namely that

$$\varepsilon_{0,\mathrm{AB}}=\varepsilon_{0,\mathrm{BA}}=\left[\varepsilon_{0,\mathrm{AA}}\,\varepsilon_{0,\mathrm{BB}}\right]^{1/2}. \quad (12)$$

The anisotropy of the interaction potential is captured by the two functions raised to the adjustable (but fixed) powers of ν and μ in Eq. (11), which tune the value of $\varepsilon_{0,ab}$ as relative molecular orientations evolve in the system. The first function is given by

$$\varepsilon_{1,ab}(\hat{\mathbf{u}}_i,\hat{\mathbf{u}}_j)=\left[1-\chi_{ab}{}^2 c_{ij}{}^2\right]^{-1/2}. \quad (13)$$

Physically, $\varepsilon_{1,ab}(\hat{\mathbf{u}}_i,\hat{\mathbf{u}}_j)$ favors a parallel alignment of discogens and promotes the formation of characteristic liquid-crystalline mesophases. The second function is defined as

$$\varepsilon_{2,ab}(\hat{\mathbf{r}}_{ij},\hat{\mathbf{u}}_i,\hat{\mathbf{u}}_j)=\Gamma(\alpha_{ab}{}',\chi_{ab}{}'), \quad (14)$$

where $\alpha_{ab}{}'$ are free parameters[148] used to tailor the attractive interactions related to the two non-equivalent tee configurations (a role analogous to that played by α_{ab}). Now,

$$\chi_{ab}{}'=\frac{(\kappa_{ab}{}')^{1/\mu}-1}{(\kappa_{ab}{}')^{1/\mu}+1}, \quad (15)$$

and

$$\kappa_{ab}{}'=\varepsilon_{ab}^{\mathrm{ee}}/\varepsilon_{ab}^{\mathrm{ff}}, \quad (16)$$

where $\varepsilon_{ab}^{\mathrm{ee}}$ is the potential well depth for an edge-edge configuration, while $\varepsilon_{ab}^{\mathrm{ff}}$ is the potential well depth for a face-face configuration. The values of $\kappa_{ab}{}'$ chosen in this work favor ff configurations over ee configurations, a feature that promotes characteristic orientationally-ordered discotic phases.

A Gay-Berne parameter set is expressed using the notation GB(κ, κ', μ, ν) proposed by Bates and Luckhurst[151]. This convention is used throughout this work. One parameterization investigated in this work is GB(0.345, 0.2, 1.0, 2.0), being of experimental relevance because it has been previously mapped to a triphenylene core[152,153].

The systems considered in this work are binary mixtures of A-type (*thin*) and B-type (*thick*) discogens. Because the B-type fluid is always present in a binary mixture with identical shape and interaction strength anisotropies, it is taken as the reference liquid component. The mixtures in this work are characterized by a bidispersity parameter,

$$q=\kappa_{\mathrm{AA}}/\kappa_{\mathrm{BB}}, \quad (17)$$

Table 1 Molecular parameters for discotic binary mixtures

Mixture	κ_{AA}	κ_{BB}	q
I	0.400	0.500	0.800
II	0.345	0.500	0.690
III	0.286	0.500	0.572

which describes the relative thickness of the two discogen species, and the concentration x_{BB}. All binary mixtures considered in this work are equimolar (i.e., $x_{\mathrm{BB}}=0.50$). Moreover, a mixture is characterized by interaction strengths $\varepsilon_{0,ab}/\varepsilon_{0,\mathrm{BB}}$, wherein $\varepsilon_{0,\mathrm{BB}}=1.0$ is held fixed.

The effect of molecular bidispersity and interaction strength was explored concomitantly in this study. More specifically, the behavior of three discogen binary mixtures was recorded and subsequently compared. Molecular parameters for each mixture are listed in Table 1. The values of q appearing in Table 1 enable a study on the stability of orientational phases as well as system homogeneity for *weakly*, *moderately*, and *strongly* bidisperse (binary) mixtures.

In addition to the molecular parameters describing a binary mixture, the corresponding model parameters for each system are summarized in Table 2. The set of $\varepsilon_{0,ab}$ for a binary mixture is somewhat arbitrary, but for simplicity and to have a point of reference, those cited in the literature for calamitic (rod-like) mesogens[86] were adopted in this work. However, it should be stressed that the bidispersity due to $\varepsilon_{0,ab}$ is comparatively weaker than the bidispersity brought on by discogen thickness.

Table 2 Model parameters for discotic binary mixtures †

Mixture	ab	$\varepsilon_{0,ab}$	χ_{ab}	α_{ab}	$\chi_{ab}{}'$
I	AA	1.316	−0.724	1.000	−0.666
	BB	1.000	−0.600	1.000	−0.666
	AB	1.147	−0.659	1.048	−0.660
	BA	1.147	−0.659	0.954	−0.660
II	AA	1.175	−0.787	1.000	−0.666
	BB	1.000	−0.600	1.000	−0.666
	AB	1.085	−0.687	1.070	−0.666
	BA	1.085	−0.687	0.934	−0.666
III	AA	1.103	−0.854	1.000	−0.666
	BB	1.000	−0.600	1.000	−0.666
	AB	1.050	−0.716	1.090	−0.660
	BA	1.050	−0.716	0.916	−0.660

† In addition to the parameters listed, $\alpha_{ab}{}'=1.000$ for all $ab\in\{\mathrm{A},\mathrm{B}\}$ in the absence of additional molecular information. Note that from the definition of χ_{ab}, positive and negative roots are possible; however, only the negative root yields a physically sound form of the intermolecular potential for discogenic mixtures. This complication is not present in α_{ab} because it enters in the model as $\alpha_{ab}{}^2$. This implies that $\alpha_{ab}{}^2>0$ from Eq. (10) given that $0<\kappa_{aa}<1$ and $0<\kappa_{bb}<1$ for a discotic mixture.

Specific limiting configurations are considered to gain insight on the interaction potential for a discotic system, as described in Fig. 1. In these cases, $\hat{\mathbf{u}}_i$ and $\hat{\mathbf{u}}_j$ attain specific values, so that the notation $U_{ab}\left(\mathbf{r}_{ij},\hat{\mathbf{u}}_i,\hat{\mathbf{u}}_j\right)$ can be simplified to $U_{ab}(r)$, with r repre-

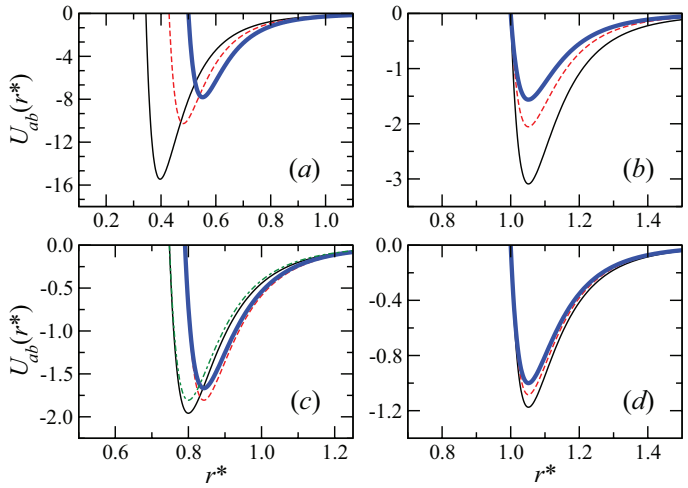

Fig. 1 Intermolecular potential contributions $U_{ab}(r^*)$ for Mixture II: AA (thin line), BB (thick line), AB (dashed line), and BA (dot-dashed line). The scalar distance r between discogens is considered in reduced units, such that $r^* = r/\sigma_{0,\mathrm{BB}}$, as discussed in Section 2.2. Shown are plots for (*a*) face-face, (*b*) edge-edge, (*c*) tee-shaped, and (*d*) cross configurations. Note that $U_{\mathrm{AB}}(r^*) = U_{\mathrm{BA}}(r^*)$ for the contributions shown in panels (*a*), (*b*), and (*d*).

senting the intermolecular distance. The set of intermolecular potentials $U_{ab}(r)$ for Mixture II is used as a representative example in Fig. 1. Note that $\kappa_{ab}{}'$ values favor strongly face-face configurations over any of the other configurations, as mentioned in the context of Eq. (16). In effect, the chosen parameter set promotes the columnar mesophase, which is characteristic of discotic systems. Moreover, note that consistent with $\alpha_{ab}{}' = 1.000$, the two tee configurations for the cross-terms [i.e., $U_{\mathrm{AB}}(r)$ and $U_{\mathrm{BA}}(r)$] have identical well depths.

2.2 Molecular Dynamics Simulations

Pure liquids and binary mixtures were modeled using MD simulations performed in the isothermal-isobaric (NPT) ensemble[154,155]. Each system (either a one-component liquid or a binary mixture) was fixed at $N = 1372$ discogens contained within an orthorhombic cell. State point variables, length scales, and time scales follow the convention of reduced units. Because the reference system in this work is the B-type liquid, all variables are referenced with respect to BB terms. Reduced units are scaled by the Boltzmann constant k_{B}, discogen diameter $\sigma_{0,\mathrm{BB}}$, discogen mass $m_{\mathrm{BB}} = 1$, and potential energy well depth $\varepsilon_{0,\mathrm{BB}}$ for the cross configuration of two B-type discogens. In this work, $m_{\mathrm{AA}} = m_{\mathrm{BB}}$ for simplicity. An arbitrary distance r_α is given in reduced units as $r_\alpha{}^* = r_\alpha/\sigma_{0,\mathrm{BB}}$. Temperature $T^* = k_{\mathrm{B}}T/\varepsilon_{0,\mathrm{BB}}$ and pressure $P^* = P\sigma_{0,\mathrm{BB}}{}^3/\varepsilon_{0,\mathrm{BB}}$ were held fixed using a Nosé-Hoover thermostat/barostat couple, with a thermostat constant $Q_{\mathrm{T}} = 10$ and a barostat constant $Q_{\mathrm{P}} = 1000$. The simulation yielded an equilibrium orthorhombic cell of dimensions $L_\gamma{}^* = L_\gamma/\sigma_{0,\mathrm{BB}}$ (with $\gamma = x,y,z$) and total volume $V^* = L_x{}^* \times L_y{}^* \times L_z{}^*$. The number density for a given system is reported as $\rho^* = \rho\sigma_{0,\mathrm{BB}}{}^3 = N/V^*$. Equations for translational and rotational motion were integrated using the velocity-Verlet algorithm with a reduced time step $\delta t^* = \delta t(\sigma_{0,\mathrm{BB}}{}^2 m_{\mathrm{BB}}/\varepsilon_{0,\mathrm{BB}})^{-1/2} = 0.0015$. The moment of inertia (for rotational motion) was calculated from[156]

$$I_{aa} = \frac{1}{20} m_{aa}\, \sigma_{0,aa}{}^2 \left(\kappa_{aa}{}^2 + 1\right) \tag{18}$$

and implemented in a simplified quaternion scheme to describe rotational motion[155,157–159]. The intermolecular potential was truncated uniformly (independent of discogen type) to optimize computational time. The interaction cutoff radius used was

$$r_{\mathrm{c}} = (\kappa_{ab,\max} + 1)\sigma_{0,ab,\max}. \tag{19}$$

For systems considered in this study, $\kappa_{ab,\max} = \kappa_{\mathrm{BB}}$, $\sigma_{0,ab,\max} = \sigma_{0,\mathrm{BB}} = 1.0$, and $r_{\mathrm{c}} = 1.6\,\sigma_{0,\mathrm{BB}}$. For the sake of simplicity, identical diameters were used for discogens of different types (i.e., $\sigma_{0,\mathrm{AA}} = \sigma_{0,\mathrm{BB}}$). Simulation runs consisted of $\mathcal{O}(10^6)$ time steps for equilibration, followed by production runs of the same order of magnitude. To minimize configurational correlations between measurements, thermodynamic and structural quantities were calculated every 50 time steps, from which averages were then determined.

2.3 Characterization of Phases

The extent of orientational order in each fluid sample was determined through $\lambda_{\max}$, defined as the largest eigenvalue obtained by diagonalizing the orientational tensor[160]

$$\mathbf{Q} = \frac{1}{2N} \sum_{i=1}^{N} \left(3\hat{\mathbf{u}}_i \otimes \hat{\mathbf{u}}_i - \mathbf{I}\right), \tag{20}$$

where $\otimes$ denotes the tensor product, $\mathbf{I}$ corresponds to the identity matrix, and N is the total number of discogens contained in the system. The director $\mathbf{n}$ is the normalized eigenvector corresponding to $\lambda_{\max}$, and $S = \lambda_{\max}$ is referred to as the *orientational order parameter*. Thus, if $S = 0$, the liquid is in an isotropic state; S increases as the number of molecular axes aligning with the director increases. An extension of Eq. (20) is used in this work to define type-resolved contributions,

$$\mathbf{Q}_{aa} = \frac{1}{2N_{aa}} \sum_{i=1}^{N_{aa}} \left(3\hat{\mathbf{u}}_i \otimes \hat{\mathbf{u}}_i - \mathbf{I}\right), \tag{21}$$

where S_{aa} is the second-rank order parameter for a-type discogens in a binary mixture. When comparing binary mixtures with pure liquids, the S_{aa} are primed for pure liquids (thus, S_{AA} is the order parameter for the A-type contribution in a mixture, whereas $S_{\mathrm{AA}}{}'$ is the order parameter for the pure A-type liquid).

To characterize the orientational and translational order of liquid-crystalline phases, two classes of (type-resolved) pair correlation functions were calculated. The parallel pair correlation function for the a-type discogen is defined as

$$g_{\parallel,aa}(r_\parallel) = \left\langle \frac{\sum_{i\neq j}^{N_{aa}} \delta\left(r_\parallel - r_{ij,\parallel}\right)\theta\left(\varsigma\sigma_{0,aa} - r_{ij,\perp}\right)}{2\pi x_{aa}{}^2 N\rho\left(\varsigma\sigma_{0,aa}\right)^2 h_\parallel} \right\rangle, \tag{22}$$

with ς representing an adjustable length-scaling factor. When $\varsigma =$

0.5, $g_{\parallel,aa}(r_\parallel)$ is more generally known as columnar pair correlation function: it probes the positional order of discogens within a column. Upon increasing ς, $g_{\parallel,aa}(r_\parallel)$ allows to probe the extent of columnar interdigitation (an effect to be addressed in Section 3). Profiles for $g_{\parallel,aa}(r_\parallel)$ are obtained as a canonical average over relevant configurations from the trajectory and $\theta(x)$ is the Heaviside step function [i.e., $\theta(x)=1$ when $x\geq 0$ and $\theta(x)=0$ otherwise]. A (solid) cylindrical volume of height $h_\parallel$ is used to scan discogens oriented along a direction parallel to $\mathbf{n}$ about a probe discogen: $r_{ij,\parallel}=|\mathbf{r}_{ij,\parallel}|=|\mathbf{r}_{ij}\cdot\mathbf{n}|$ is the center-of-mass separation of a discogen along the director $\mathbf{n}$ and $r_{ij,\perp}=|\mathbf{r}_{ij,\perp}|=|\mathbf{r}_{ij}-\mathbf{r}_{ij,\parallel}|$ is the transversal separation from $\mathbf{n}$. The mole fraction of the a-type discogen is given by x_{aa} for a binary mixture comprised of N *total* discogens at a *bulk* number density ρ. For most calculations involving $g_{\parallel,aa}(r_\parallel)$, $\varsigma=0.5$ and $h_\parallel=0.01\sigma_{0,aa}$ were used.

The perpendicular pair correlation function is defined as

$$g_{\perp,aa}(r_\perp)=\left\langle\frac{\sum_{i\neq j}^{N_{aa}}\delta\left(r_\perp-r_{ij,\perp}\right)\theta\left(\delta L_\perp-r_{ij,\parallel}\right)}{4\pi {x_{aa}}^2 N\rho r_\perp\delta L_\perp h_\perp}\right\rangle, \tag{23}$$

where concentric cylinders of width $\delta L_\perp$ and height $h_\perp$ are used to probe the translational structure in a volumetric region perpendicular to $\mathbf{n}$ with respect to a probe discogen. For calculations involving $g_{\perp,aa}(r_\perp)$, $h_\perp=\kappa_{aa}\sigma_{0,aa}$ and $\delta L_\perp=0.01\sigma_{0,aa}$ were used.

To probe the formation of a-rich domains and liquid interfaces in the mixture, type-resolved concentration profiles were monitored as a function of position r_γ with respect to the simulation cell along a specific direction ($\gamma=x,y,z$), defined as

$$\varphi_{aa}(r_\gamma)=\frac{\rho_{aa}(r_\gamma)}{\rho_{\mathrm{AA}}(r_\gamma)+\rho_{\mathrm{BB}}(r_\gamma)}. \tag{24}$$

Note that the γ chosen for $\varphi_{aa}(r_\gamma)$ is inconsequential, so long as the interfaces between A-rich and B-rich domains are predominantly orthogonal to γ, so as to enable the identification of type-rich domains. Now, $\varphi_{aa}(r_\gamma)$ is defined in terms of local densities,

$$\rho_{aa}(r_\gamma)=\frac{N_{aa}(r_\gamma)}{A_\gamma H}, \tag{25}$$

where $N_{aa}(r_\gamma)$ is the number of a-type discogens in a thin slice of width Δr_γ centered about r_γ, A_γ is the area probed orthogonal to the direction γ (i.e., it is the base of the "probing box"), and H is the height of the "probing box". For these calculations, $\Delta r_\gamma=0.05\sigma_{0,\mathrm{BB}}$ was used.

To investigate the extent of demixing in a binary mixture, the conventional (three-dimensional) radial distribution function was computed, using the generalization for type-resolved contributions [161], given by

$$g_{ab}(r)=\left\langle\frac{\sum_{i=1}^{N_{aa}}\sum_{j=1}^{N_{bb}}\delta\left(r-r_{ij}\right)\left(1-\delta_{ab}\delta_{ij}\right)}{8\pi x_{aa}x_{bb}N\rho r^2\Delta r}\right\rangle, \tag{26}$$

where Δr represents the thickness of a spherical shell of radius r, while δ_{ab} and δ_{ij} are Kronecker delta functions. For most of the calculations performed in this work, $\Delta r=0.01$ was used.

Concentration-concentration fluctuations were probed in the system by summing the set of $g_{ab}(r)$ as

$$g^{\varphi\varphi}(r)=g_{\mathrm{AA}}(r)+g_{\mathrm{BB}}(r)-2g_{\mathrm{AB}}(r), \tag{27}$$

in which each $g_{ab}(r)$ is normalized to unity as $r\to\infty$. For a homogeneous (uniformly mixed) sample, $g^{\varphi\varphi}(r)=0$ for all r. When demixing occurs, $g^{\varphi\varphi}(r)\neq 0$ for a characteristic range of r: this allows for the identification of length scales where the system is heterogeneous, in the sense that there exist A-rich and B-rich domains, *locally* and/or *globally* in the sample [161]. In a convenient manner, $g^{\varphi\varphi}(r)>0$ when self-contacts (i.e., AA and BB) dominate, while $g^{\varphi\varphi}(r)<0$ when cross-contacts (i.e., AB and BA) become significant.

3 Results and Discussion

3.1 Single-Component Discogen Systems

In order to account for the effects that discogen mixtures have on phase stability and liquid structure, one-component (pure) samples of *thin* [i.e., GB(0.345,0.2,1.0,2.0)] and *thick* [i.e., GB(0.500,0.2,1.0,2.0)] discogens were prepared as representative systems. The volumetric (T^*-ρ^*) phase diagram of the *thin* discogen has been reported in the literature [147]. Those results are extended in this work by providing the pressure-temperature (P^*-T^*) phase diagrams of both *thin* and *thick* discogen systems, shown in Fig. 2. For ease of comparison with prior work, the interaction strength parameter for pure samples was set to $\varepsilon_{0,\mathrm{AA}}=\varepsilon_{0,\mathrm{BB}}=1.0$ (i.e., A-type refers to the *thin*-discogen pure liquid, whereas B-type refers to the *thick*-discogen pure liquid).

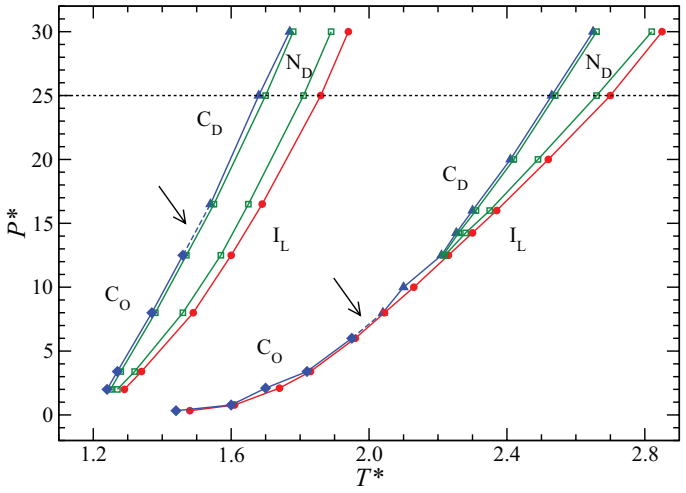

Fig. 2 Pressure-temperature (P^*-T^*) phase diagrams for two pure systems: $\kappa_{\mathrm{AA}}=0.345$, $\varepsilon_{0,\mathrm{AA}}=1.00$ as the *thin*-discogen sample (right) and $\kappa_{\mathrm{BB}}=0.500$, $\varepsilon_{0,\mathrm{BB}}=1.00$ as the *thick*-discogen sample (left). Lines serve as a guide to the eye and denote limits of phase stability. Shown are boundary regions for isotropic liquid ($\mathrm{I_L}$, circles), discotic nematic ($\mathrm{N_D}$, squares), disordered columnar ($\mathrm{C_D}$, triangles), and ordered columnar ($\mathrm{C_O}$, diamonds) phases. Arrows and dashed segments highlight state-point ranges where the $\mathrm{C_D}$-$\mathrm{C_O}$ crossover is expected. The isobar used in this work ($P^*=25.0$) is highlighted (dotted line).

Points shown in Fig. 2 were collected from temperature sweeps done in steps of $\Delta T^*=0.01$ for a given pressure P^*. An isotropic

configuration of discogens (at high temperature) was cooled under isobaric conditions to produce the characteristic phases for a given system. This procedure was repeated for different pressures, ranging from $P^* = 0.330$ to $P^* = 30.0$. It is important to note that the boundaries in Fig. 2 represent limits of phase stability and *do not* correspond to coexistence lines. This is because simulations in the (NPT)-ensemble can probe thermodynamic state points inaccessible by conventional (NVT)-ensemble simulations, without yielding phase separation or coexistence.

Phase diagrams for *thin* and *thick* discogens share a few common features. For instance, a nematic (N_D) phase "bay" separates state-point domains corresponding to isotropic and columnar phases [162]. In addition, the disordered (hexagonal) columnar (C_D) phase is favored at higher pressures ($P^* \geq 8.0$ for the *thin* discogen and $P^* \geq 16.5$ for the *thick* discogen), while an ordered (rectangular) columnar (C_O) phase is observed at lower pressures ($P^* \leq 6.0$ for the *thin* discogen and $P^* \leq 12.5$ for the *thick* discogen) [163]. However, there exists an important distinction between the two topologies: a critical point is observed for the *thick*-discogen sample when $P^* = 0.15$ (not shown in Fig. 2), which leads to an isotropic liquid-gas (I_L-I_G) transition. A similar critical point is not observed for the thin-discogen system. The values $\kappa = 0.345$ and $\kappa = 0.500$ represent parameterization signposts in the sense that as κ increases (decreases), the phase behavior of the system will resemble that of the left (right) phase diagram shown in Fig. 2. Shown in Fig. 3 are characteristic molecular arrangements for the N_D [Fig. 3(a)] and C_D [Fig. 3(b)] phases. Additionally, columnar mesophases can exhibit a mobility constraint known as interdigitation, illustrated in Fig. 3(c). This effect is addressed when discussing results for the binary DLC mixtures.

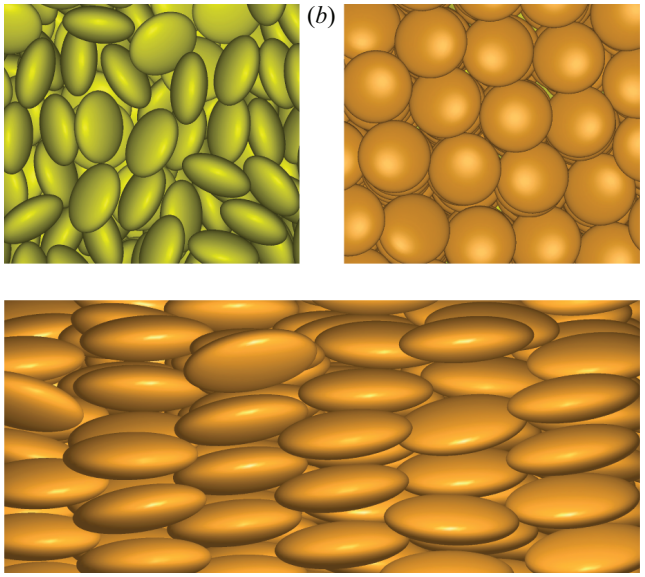

Fig. 3 Characteristic molecular arrangements for different phases observed in pure systems and mixtures. (a) A region showing the *paranematic*-like phase (B-type discogens in Mixture III when $T^* = 2.20$) [164]. (b) A region of the disordered (hexagonal) columnar phase (A-type discogens in Mixture III when $T^* = 2.20$). (c) A detailed view of interdigitation in the disordered (hexagonal) columnar phase (A-type discogens in Mixture II when $T^* = 1.95$). All simulation snapshots presented in this work were generated with QMGA [165].

3.2 Discotic Binary Mixtures

Three binary mixtures of discogens were investigated with varying extents of bidispersity q: *weak* ($q = 0.800$), *moderate* ($q = 0.690$), and *strong* ($q = 0.572$). In all cases, the reference system was taken to be the B-type (thick) discogen (with fixed $\kappa_{BB} = 0.500$). The molecular thickness of the other (A-type) discogen was varied (such that $\kappa_{AA} < 0.500$). Molecular and model parameters are listed in Table 1 and Table 2, respectively.

Studies on phase stability in the binary mixtures were all performed at $P^* = 25.0$. For this value of P^*, phase diagrams for the GB$(\kappa, 0.2, 1.0, 2.0)$ discogen capture characteristic liquid phases over a reasonably wide range of temperatures. This feature enables one to probe any induced liquid-phase stability in the presence of another component in the mixture. Moreover, reference pure systems (in Fig. 2) display homogeneous dynamics [147] and produce the same sequence of phases upon cooling: isotropic, nematic, and disordered columnar ($I_L \rightarrow N_D \rightarrow C_D$) phases when $P^* = 25.0$. There is also a range of temperatures for which the B-type pure liquid is *still* in an isotropic (i.e., I_L) phase when the A-type pure liquid is *already* in a structurally-ordered (i.e., C_D) phase. Given these differences in phase behavior, comparisons between pure systems and binary mixtures can be more readily tied to effects that arise by virtue of a mixed system.

In the following subsections, each mixture is treated separately. Comparisons of thermodynamic as well as structural properties are made between the mixture and the corresponding pure components. Pure samples were simulated with interaction strength parameters $\varepsilon_{0,aa}$ set to those of the corresponding mixture, as listed in Table 2. For example, $\varepsilon_{0,AA} = 1.31$ for Mixture I; the same interaction strength was used when simulating the pure A-type (*thin*-discogen) liquid.

3.2.1 Mixture I: Weakly Bidisperse.

An important feature of Mixture I is that it presents the smallest extent of bidispersity ($q = 0.800$) of the systems studied, with relatively thick discogens ($\kappa_{AA} = 0.400$). The stability of liquid-crystalline phases as a function of temperature T^* is probed through the orientational order parameter $S(T^*)$: the behavior emerging from the mixture as a whole [denoted $S_{tot}(T^*)$], the behavior arising from each component in the mixture [$S_{AA}(T^*)$ and $S_{BB}(T^*)$, which are type-resolved with respect to $S_{tot}(T^*)$], and the behavior of each component as a pure liquid [denoted $S_{AA}'(T^*)$ and $S_{BB}'(T^*)$ [166]]. All $S(T^*)$ variants are shown in Fig. 4.

A discontinuity in $S(T^*)$ indicates a phase transition in the liquid structure. Two transitions can be identified for Mixture I upon cooling in Fig. 4. The first discontinuity occurs at $T^* \approx 2.35$ and corresponds to an I_L-N_D phase transition. The N_D phase in the mixture originates from the nematization of both components [as inferred from the behavior of $S_{AA}(T^*)$ and $S_{BB}(T^*)$]. The other transition occurs at $T^* \approx 2.10$, which yields an N_D-C_D transition. From the behaviors of $S_{AA}(T^*)$ and $S_{BB}(T^*)$, it is evident that both components yield the C_D phase in the mixture.

Orientational transitions in the mixture occur at T^* values intermediate those of the corresponding pure liquids, due to en-

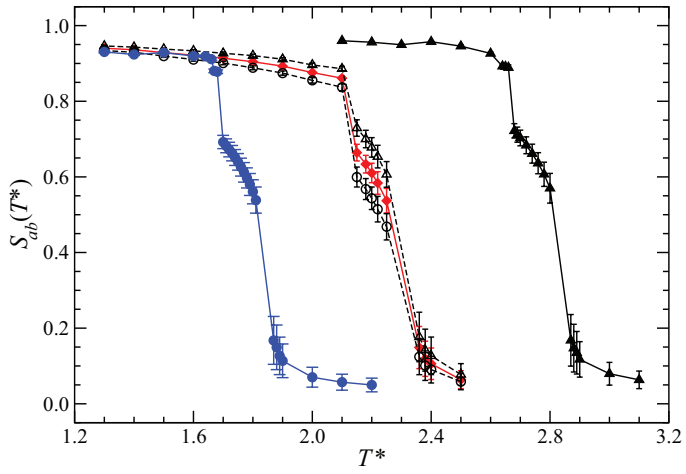

Fig. 4 Temperature-dependent orientational order parameter $S_{ab}(T^*)$ for Mixture I ($q = 0.800$, $P^* = 25.0$). Plotted are data for the mixture [$S_{\mathrm{tot}}(T^*)$, diamonds], type-resolved contributions from the mixture [$S_{\mathrm{AA}}(T^*)$, open triangles and $S_{\mathrm{BB}}(T^*)$, open circles], and corresponding pure liquids [$S_{\mathrm{AA}}{}'(T^*)$, filled triangles and $S_{\mathrm{BB}}{}'(T^*)$, filled circles].

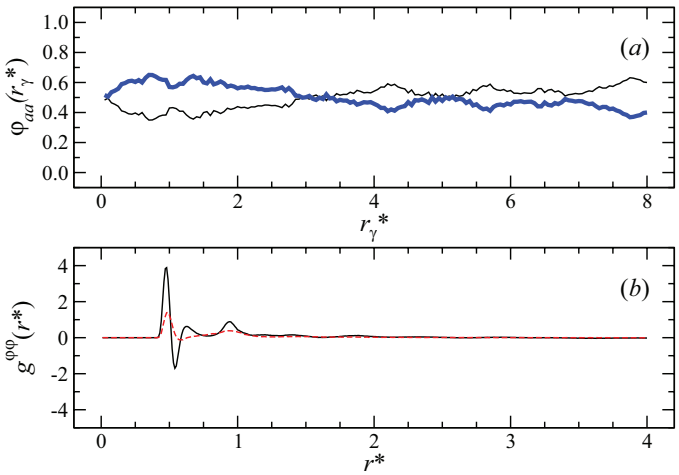

Fig. 5 Concentration-related response functions for Mixture I. (*a*) Concentration profile $\varphi_{aa}(r_\gamma{}^*)$ when $T^* = 2.10$: $\varphi_{\mathrm{AA}}(r_\gamma{}^*)$ (thin line) and $\varphi_{\mathrm{BB}}(r_\gamma{}^*)$ (thick line). (*b*) Concentration-concentration fluctuations $g^{\varphi\varphi}(r^*)$ when $T^* = 2.20$ (dashed line) and when $T^* = 2.10$ (solid line).

thalpic and entropic contributions. On the grounds of interaction strengths alone, the A-type fluid would be expected to display more structured liquid phases at higher T^* because the interaction potential has a deeper well depth (i.e., $\varepsilon_{0,\mathrm{AA}} > \varepsilon_{0,\mathrm{BB}}$). This is in fact observed when comparing the pure liquids, upon inspecting $S_{\mathrm{AA}}{}'(T^*)$ and $S_{\mathrm{BB}}{}'(T^*)$. However, the onset of ordered phases occurs at lower (higher) T^* for the A component (B component) in the mixture with respect to the pure liquids. This suggests that A-type discogens stabilize the B-type liquid through AB interactions (i.e., an enthalpic effect). Another (weak) effect develops when the nematic phase emerges: the A component is slightly more structured [$S_{\mathrm{AA}}(T^*) > S_{\mathrm{AA}}{}'(T^*)$] than the B component [$S_{\mathrm{BB}}(T^*) < S_{\mathrm{BB}}{}'(T^*)$] when comparing the centroids of data points for the $\mathrm{N_D}$ phase in Fig. 4. On a local length scale, a B-type discogen cannot interact persistently with other B-type discogens to produce a more ordered $\mathrm{N_D}$ phase due to thermal fluctuations (for B-type discogens, T^* is higher than required for the $\mathrm{N_D}$ phase). Moreover, the spatial arrangement of B-type discogens is disturbed by A-type "microdomains" (on the length scale of $\approx 0.5\sigma_{0,\mathrm{AA}}$), which can hold up in a more ordered manner (for A-type discogens, T^* is lower than required for the $\mathrm{N_D}$ phase to emerge). This interplay of spatial entropic contributions partially drives the orientational behavior of components in the mixture.

The slight bidispersity of Mixture I results in an overall weakly fractionated system. The concentration profile $\varphi_{aa}(r_\gamma{}^*)$ in Fig. 5(*a*) when $T^* = 2.10$ (corresponding to $\mathrm{C_{D,AA}}$ and $\mathrm{C_{D,BB}}$ phases) is characterized by a weak ondulatory form about the average mixture concentration, indicating that no evident interface forms. Also shown is the concentration-concentration fluctuation function $g^{\varphi\varphi}(r^*)$ in Fig. 5(*b*): when $T^* = 2.20$ (corresponding to $\mathrm{N_{D,AA}}$ and $\mathrm{N_{D,BB}}$ phases), the sample shows a highly localized response consistent with a sample in which the components remain mixed. When $T^* = 2.10$ (corresponding to $\mathrm{C_{D,AA}}$ and $\mathrm{C_{D,BB}}$ phases), $g^{\varphi\varphi}(r^*)$ shows signs of microheterogeneities, an effect that vanishes for $r^* \gtrsim 1.5$. This weakly-segregated behavior is sustained by the spatial entropic contributions governing the relative stability of the $\mathrm{N_D}$ phase in the mixture, as mentioned previously in the context of $S(T^*)$. Another indication of the weakly-segregated nature of the mixture can be gleaned from a simulation snapshot [see Fig. 6(*a*)]: A-type and B-type discogens show signs of microsegregation. In the low-temperature range ($T^* \lesssim 1.8$), the values of $S_{\mathrm{AA}}(T^*)$ and $S_{\mathrm{BB}}(T^*)$ are nearly equal.

A practical feature of Mixture I is the ability to trigger an orientationally-ordered component whose corresponding pure liquid *still* yields an isotropic state. Specifically, Fig. 4 reveals that for the B-type discogen, the $\mathrm{C_D}$ phase is observed in the mixture at $T^* \approx 2.10$, a warmer temperature than the $T^* \approx 1.70$ required in the pure B-type liquid. This reflects a widening of the T^* range, in which it is possible to induce the formation of a columnar mesophase through a DLC mixture.

3.2.2 Mixture II: Moderately Bidisperse.

For Mixture II, the A-type discogen is mapped to a triphenylene core (with $\kappa_{\mathrm{AA}} = 0.345$)[152,153] and the mixture is moderately bidisperse ($q = 0.690$). The behavior of $S(T^*)$ is shown in Fig. 7. When $T^* \approx 2.45$, an $\mathrm{I_L}$-$\mathrm{N_D}$ phase transition occurs in the mixture. In the range $2.30 \lesssim T^* \lesssim 2.45$, *prenematic*-like states emerge: A-type and B-type discogens exhibit a gradual and smooth growth for $0.2 \lesssim S(T^*) \lesssim 0.5$ (a behavior to be contrasted with the abrupt $\mathrm{I_L}$-$\mathrm{N_D}$ transition observed for Mixture I). This effect arises because the plausible ordering of A-type discogens is hampered by the presence of disordered B-type discogens and becomes pronounced when the mixture is only weakly demixed [i.e., as inferred from the likeness in behavior between $S_{\mathrm{AA}}(T^*)$ and $S_{\mathrm{BB}}(T^*)$ when $2.30 \lesssim T^* \lesssim 2.45$]. This pretransitional effect (referred to in this work as *prenematic*-like) is similar to that observed in computer simulations of binary mixtures of calamitic mesogens with presmectic ordering in the nematic phase[167,168] and in measurements of DLC flexoelectricity[64]. Also, the weakly demixed condition of *prenematic*-like state points is analogous to the mixed nematic samples observed in calamitic liquid crystals[86]. The anal-

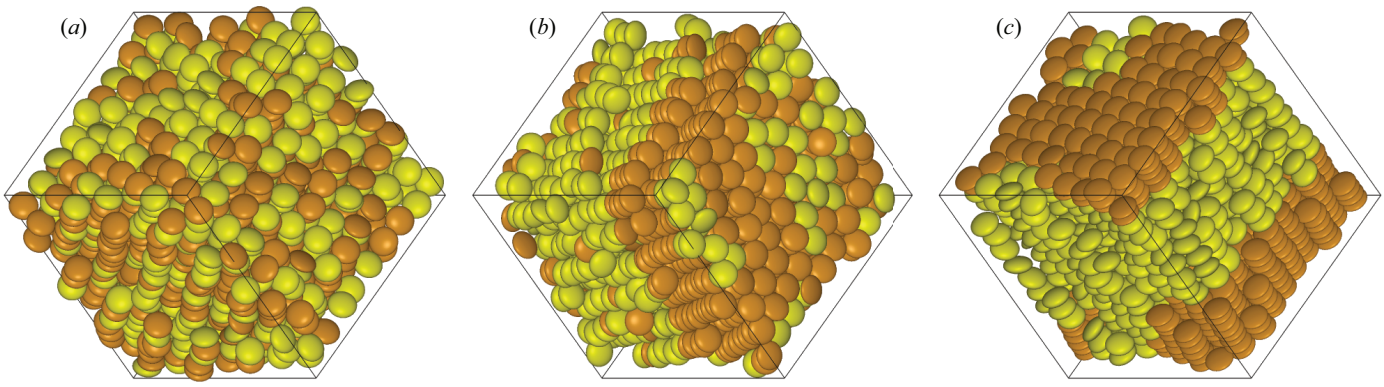

Fig. 6 Snapshots of mixtures considered in the study. Discogens are colored by type, A-type (darker, thinner) and B-type (lighter, thicker) discogens. (*a*) *Weakly* bidisperse system (Mixture I) when $T^* = 2.10$. (*b*) *Moderately* bidisperse system (Mixture II) when $T = 1.95$. (*c*) *Strongly* bidisperse system (Mixture III) when $T^* = 1.80$.

ogy between these systems and Mixture II is that orientational frustration due to molecular bidispersity results in sluggish orientational phase transitions (in this case, the I_L-N_D transition).

A discontinuity in $S(T^*)$ is observed in the mixture when $T^* \approx 1.95$, corresponding to an N_D-C_D phase transition. At this temperature, the system has segregated into two domains, each rich in one component ($C_{D,AA}$ and $C_{D,BB}$). The snapshot in Fig. 6(*b*) highlights the phase separation of the mixture. At comparable system conditions, the pure B-type liquid presents an I_L phase. The difference in temperature (i.e., $\Delta T \approx 0.27$) between the appearance of the columnar phase in the mixture ($C_{D,BB}$) and in the pure B-type liquid ($C_{D,BB}'$) reflects a convenient induction of the columnar mesophase in the system: the $C_{D,BB}$ phase is observed at higher T^* with respect to the pure B-type liquid.

The profiles for $\varphi_{aa}(r_\gamma^*)$ in Fig. 8(*a*) when $T^* = 1.95$ (corresponding to $C_{D,AA}$ and $C_{D,BB}$ mesophases) show two clearly distinct domains for A-type and B-type discogens, suggesting that the mixture has segregated. The tendency that $\varphi_{aa}(r_\gamma^*) \to 1$ for each component (in its corresponding range of r_γ^* values) corroborates the nearly complete segregation of the mixture. The profiles are asymmetric in r_γ^* despite an equimolar composition for the sample: this suggests "tighter" columnar packing for A-type discogens (spanning roughly $\Delta r_\gamma^* \approx 3$) when compared to B-type discogens (spanning roughly $\Delta r_\gamma^* \approx 5$).

The profile for $g^{\varphi\varphi}(r^*)$ in Fig. 8(*b*) when $T^* = 2.20$ is a strong indicator for segregation in the mixture, and in particular a $C_{D,AA}$-$N_{D,BB}$ coexistence. The heterogeneous nature of the mixture is corroborated by the behavior of $g^{\varphi\varphi}(r^*)$: the weak anticorrelation [i.e., $g^{\varphi\varphi}(r^*) < 0$] establishes that AB contacts are disfavored over AA and BB contacts, a condition associated with demixing. When compared to Mixture I, AA and BB contacts are seen to be more strongly favored (by higher amplitudes overall) for larger length scales [cf. Fig. 5(*b*)]. This implies relatively large domains rich in A-type or B-type discogens, consistent with the demixed state of the sample already for $T^* \approx 2.20$. Upon further cooling (when $T^* \approx 1.95$, corresponding to $C_{D,AA}$ and $C_{D,BB}$ mesophases) the sample displays slightly larger amplitudes and sharper features in $g^{\varphi\varphi}(r^*)$, but with a similar profile overall.

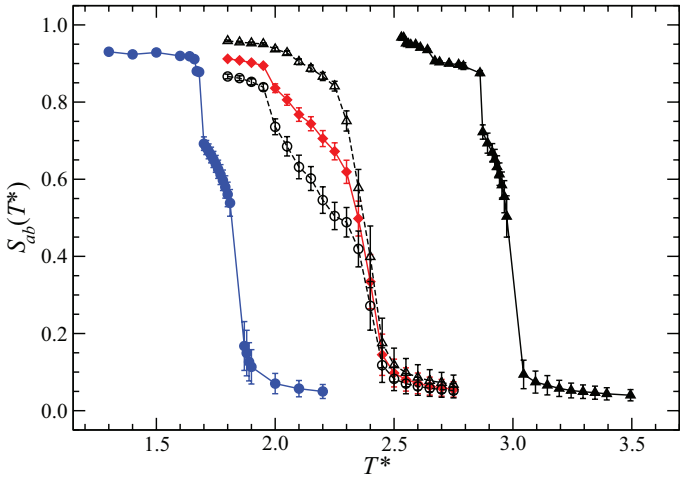

Fig. 7 As in Fig. 4, but for Mixture II ($q = 0.690$, $P^* = 25.0$).

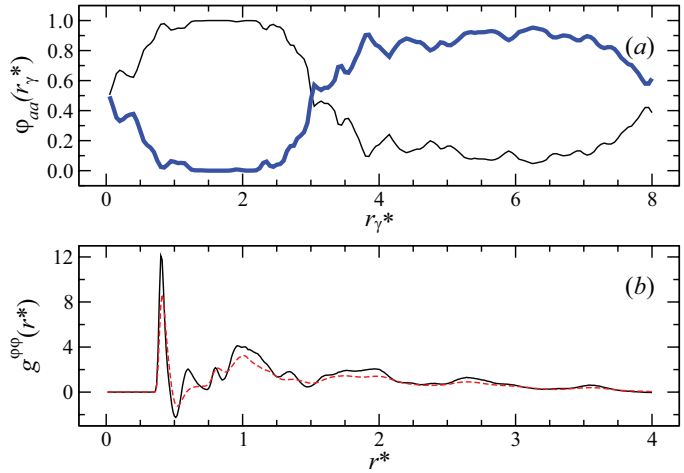

Fig. 8 As in Fig. 5, but for Mixture II. (*a*) $\varphi_{aa}(r_\gamma^*)$ when $T^* = 1.95$. (*b*) $g^{\varphi\varphi}(r^*)$ when $T^* = 2.20$ (dashed line) and when $T^* = 1.95$ (solid line).

The tighter packing of A-type discogens, as mentioned previously in the context of Fig. 8(*a*), suggests that a composition phase diagram (e.g., T^* against x_{AA}) will also be asymmetric.

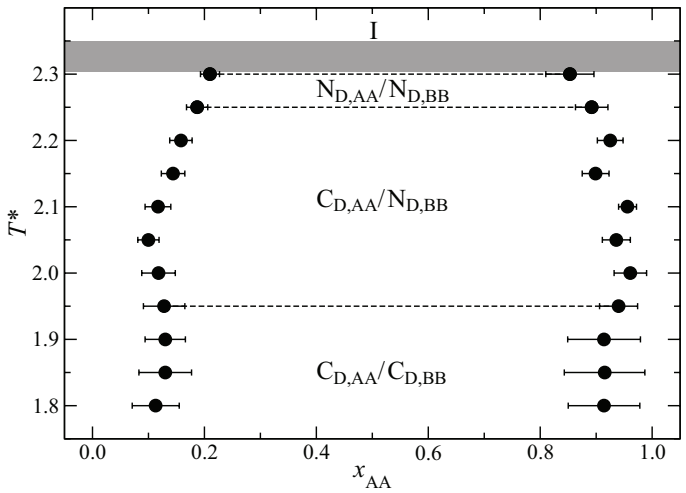

Fig. 9 Temperature-composition phase diagram for Mixture II ($q = 0.690$, $P^* = 25.0$). The dotted isotherms separate coexistence types in the two-phase region [e.g., the $C_{D,AA}/N_{D,BB}$ label denotes the fraction of A-type discogens in the $N_{D,BB}$ phase (left data points) and in the $C_{D,AA}$ phase (right data points)]. The grayed region corresponds to the approximate temperature range for the *prenematic*-like phase.

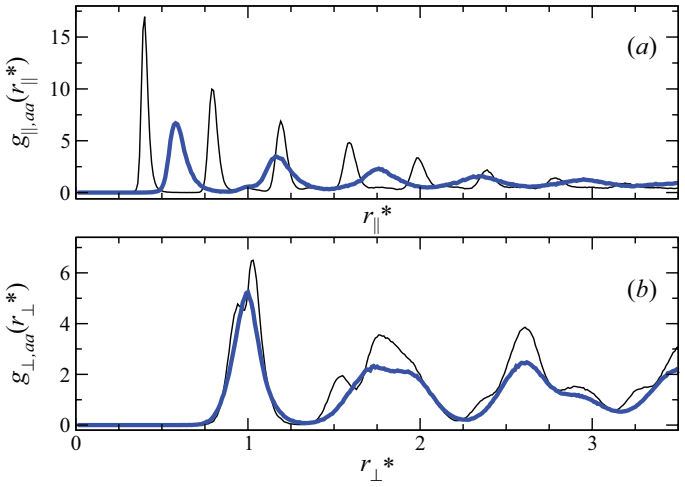

Fig. 10 Pair correlation functions for Mixture II when $T^* = 1.95$: (*a*) parallel contribution $g_{\parallel,aa}(r^*)$ and (*b*) perpendicular contribution $g_{\perp,aa}(r^*)$. Data are resolved according to discogen type: A component (thin line) and B component (thick line).

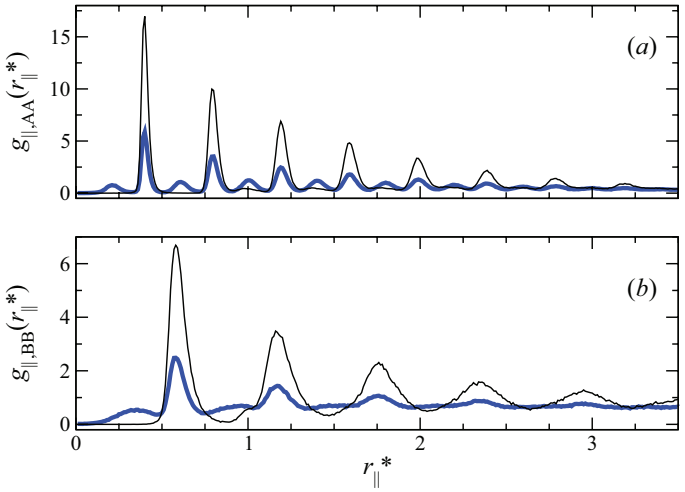

Fig. 11 Study on the extent of interdigitation as probed by parallel correlation functions $g_{\parallel,aa}(r_\parallel^*)$ for a probe radius adjusted with $\varsigma = 0.50$ (thin line) and $\varsigma = 0.85$ (thick line) for Mixture II when $T^* = 1.95$. Data are resolved by discogen-type contributions: (*a*) A type and (*b*) B type. Interdigitation is evident for $\varsigma = 0.85$, as indicated by the emergence of secondary, lower-amplitude peaks appearing between main peaks (i.e., those captured when $\varsigma = 0.50$).

A representative composition phase diagram is shown in Fig. 9, obtained by averaging $\mathcal{O}(10^1)$ configuration snapshots [each obtained after $\mathcal{O}(10^5)$ simulation time steps] over the last $\mathcal{O}(10^6)$ simulation time steps. Although noise in the data set yields a rather qualitative trace, slight asymmetric demixing behavior is discernible for the mixture. Also indicated in Fig. 9 are the coexistence regimes in the phase diagram.

The liquid structure of A-type and B-type discogens in the mixture was probed with $g_{\parallel,aa}(r_\parallel{}^*)$ and $g_{\perp,aa}(r_\perp{}^*)$, as shown in Fig. 10, for the columnar mesophase in the segregated state. Oscillations in $g_{\parallel,aa}(r_\parallel{}^*)$ [refer to Fig. 10(*a*)] suggest that A-type and B-type discogens form disordered (hexagonal) columnar phases, as confirmed by a simulation snapshot [see Fig. 6(*b*)]. This behavior is expected because the ordered (rectangular) columnar phase (C_O) in pure systems is less stable at higher pressures and temperatures. Given the present system conditions (in particular, $P^* = 25.0$), the system stabilizes by packing into a "relaxed" C_D phase[147]. Furthermore, correlation functions for the mixture have peaks of different amplitude, separated by $\Delta r_\parallel{}^* \approx 0.40$ and $\Delta r_\parallel{}^* \approx 0.58$ in $g_{\parallel,AA}(r_\parallel{}^*)$ and $g_{\parallel,BB}(r_\parallel{}^*)$, respectively. Therefore, A-type discogens tend to yield more tightly packed columns when compared to B-type discogens. The behavior of $g_{\perp,AA}(r_\perp{}^*)$ and $g_{\perp,BB}(r_\perp{}^*)$ [refer to Fig. 10(*b*)] reveals a characteristic hexagonal structure due to the splitting of the second peak[152,153,169] when $r_\perp{}^* \approx 1.59$ (broadly and weakly so for the B-type sample). The splitting in the first peak for $g_{\perp,AA}(r_\perp{}^*)$ (when $r_\perp{}^* \approx 1$) is attributed to columnar interdigitation[152,169], a spatial constraint produced when neighboring columns interlock through the interstices of cylindrically-stacked discogens[147] [cf. Fig. 3(*c*)].

Columnar packing was explored further by interrogating the sample for the extent of interdigitation in each component [refer to Fig. 3(*c*) for a molecular view of this effect]. This was accomplished through $g_{\parallel,aa}(r_\parallel{}^*)$ for an increasing "probe volume": specifically, the probe volume was adjusted by increasing ς, as defined in Eq. (22). The results for this study are reported in Fig. 11. As ς increases, one captures the interdigitation effect more clearly: secondary peaks emerge between major (higher-amplitude) peaks in $g_{AA}(r_\parallel{}^*)$ [refer Fig. 11(*a*)] and $g_{BB}(r_\parallel{}^*)$ [refer Fig. 11(*b*)]. This suggests that A-type and B-type discogens slip into the voids of neighboring columns (within columns of A-dominant or B-dominant regions). Moreover, $g_{\parallel,BB}(r_\parallel{}^*)$ is broader and of lower amplitude than $g_{\parallel,AA}(r_\parallel{}^*)$, indicating that the B-type liquid is more disordered and less compact than the corresponding A-type liquid: this leads to weaker interdigitation in the B-type domain. A transversal view from the sample showing these effects appears in Fig. 6(*b*).

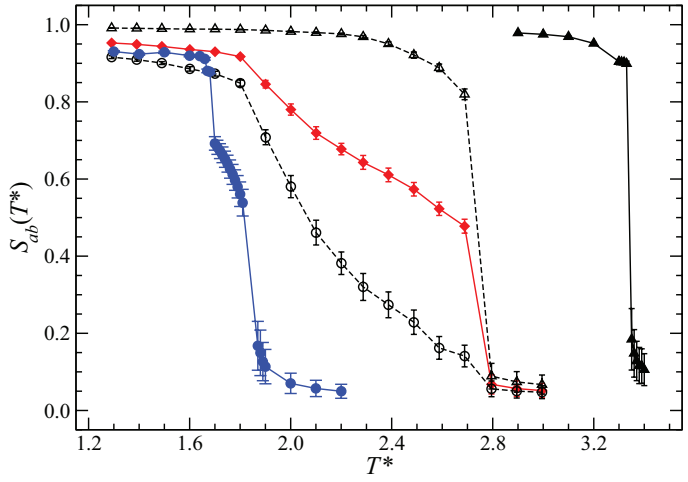

Fig. 12 Same as in Fig. 4, but for Mixture III ($q = 0.572$, $P^* = 25.0$).

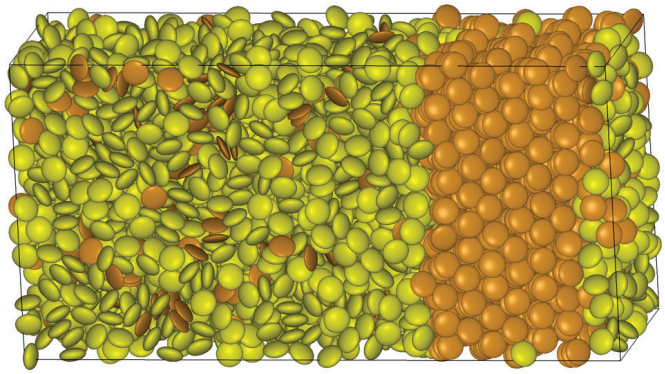

Fig. 13 As in Fig. 6, but for Mixture III when $T^* = 2.70$, showing the coexistence of $C_{D,AA}$ and $I_{L,BB}$ phases. This state point shows signs of nearly complete demixing (i.e., segregation).

3.2.3 Mixture III: Strongly Bidisperse.

The most bidisperse system in the study is Mixture III ($q = 0.572$), which contains a relatively thin discogen ($\kappa_{AA} = 0.286$). A striking feature of the pure A-type liquid is that the C_D phase is strongly favored without the liquid having to first undergo nematization (at least for $P^* = 25.0$). This contrasts with the referential B-type liquid, which displays the sequence $I_L \rightarrow N_D \rightarrow C_D$. Consequently, it is of interest to consider the manner in which the A-type liquid influences the orientational properties of the mixture as captured by $S(T^*)$ (see Fig. 12).

Because the A-type discogen (as a pure liquid, with $\kappa_{AA} = 0.286$) can undergo an I_L-C_D transition without nematization, this trait is seen to carry over in Mixture III. When the $I_{L,AA}$ phase is no longer stable due to cooling ($T^* \lesssim 2.70$), the sample segregates to yield a $C_{D,AA}$ mesophase in coexistence with a complex, N_D-like mesophase. Type-resolved contributions of $S(T^*)$ indicate a sluggish growth and that the N_D-like behavior of the B component is prompted by the presence of an ordered "layer" of B-type liquid adjacent to a $C_{D,AA}$ domain, along with a disordered B-type bulk phase away from the A-type/B-type interface. This *paranematic*-like (*para*-N_D) phase is likened to the ordering of liquid-crystalline particles around a colloid[170,171] or the surface layering prompted by confinement and/or an induced field[172–175]. It is stressed that the *para*-N_D ordering in the present case *is not* a consequence of an applied field or confinement. Rather, the analogy lies in that the A-type phase imposes a "field" which "communicates" orientational order to an adjacent "layer" of B-type discogens. This leads to enhanced orientational order at the interface of two molecular types, as is similarly observed in certain liquid-crystalline mixtures, with[176] or without[177] an applied field.

Once the A-type liquid segregates from the mixture to form a $C_{D,AA}$ phase, there is no evident discontinuity in $S(T^*)$ for the B-type liquid: $S(T^*)$ simply increases gradually and smoothly, passing through N_D values, until the response levels off when the system forms a columnar mesophase. Before the response in $S(T^*)$ plateaus, approximately three phase regions can be identified: an $I_{L,BB}$-$C_{D,AA}$ coexistence for $2.35 \lesssim T^* \lesssim 2.70$, a *para*-$N_{D,BB}$-$C_{D,AA}$ coexistence for $2.00 \lesssim T^* \lesssim 2.35$, and a $N_{D,BB}$-$C_{D,AA}$ coexistence for $1.80 \lesssim T^* \lesssim 2.00$. The widening of temperature ranges for nematic-like state points due to strong mixture bidispersity has also been observed in calamitic samples[86,178,179]. The coexistence of the $I_{L,BB}$-$C_{D,AA}$ liquid can be appreciated from the simulation snapshot shown in Fig. 13: the B-type liquid assumes an isotropic-like phase, while the A-type liquid yields a $C_{D,AA}$ phase.

When the system reaches $T^* \approx 1.80$, two independent bulk-like columnar phases are produced (i.e., one of A-type discogens and the other of B-type discogens). This arrangement is supported by the simulation snapshot shown in Fig. 6(c). Under these conditions, the A component (as inferred from the centroids of data points) displays slightly greater orientational order when compared to the pure liquid. Moreover, the A-rich and B-rich domains possess nearly identical values for $S(T^*)$. It is worth noting that at the same T^*, the pure B-type liquid exhibits an N_D phase which contrasts with the $C_{D,BB}$ phase of the mixture.

The segregated nature of the mixture is also confirmed by the response in $\varphi_{aa}(r_\gamma{}^*)$ and $g^{\varphi\varphi}(r^*)$. The response shown by $\varphi_{aa}(r_\gamma{}^*)$ in Fig. 14(a) indicates that A-type discogens are practically absent in B-type domains, suggesting that the sample has nearly segregated completely. Moreover, $g^{\varphi\varphi}(r^*)$ in Fig. 14(b) shows a non-zero response for practically all radial length scales, consistent with the segregated state of the mixture. Comparing the temperatures shown for $g^{\varphi\varphi}(r^*)$, it is clear that the $C_{D,AA}$-*para*-$N_{D,BB}$ coexistence (when $T^* \approx 2.20$) occurs with nearly complete segregation; further cooling of the sample to yield the $C_{D,AA}$-$C_{D,BB}$ coexistence (when $T^* \approx 1.80$) does not modify $g^{\varphi\varphi}(r^*)$ significantly.

Mixture III displays an increased temperature range ($\Delta T^* \approx 0.35$) in which states emerge with *para*-N_D-like behavior: an ordered "layer" of B-type liquid coexists with a disordered (weakly nematic) B-type bulk region. This behavior is coupled to a globally-segregated sample, where the A component weakly induces the columnar mesophase in the B-type liquid. As a result, the induced mesophase appears at a temperature that closely resembles the behavior of the pure B-type liquid (i.e., $\Delta T^* \approx 0.12$). In effect, the strong bidispersity of Mixture III weakens the ability of the A-type discogen to induce an ordered columnar mesophase in the B-type liquid.

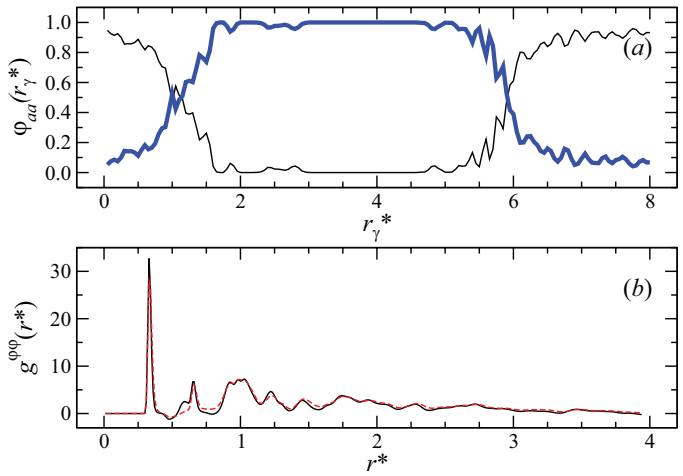

Fig. 14 As in Fig. 5, but for Mixture III. (*a*) $\varphi_{aa}(r_\gamma^*)$ when $T^* = 1.80$. (*b*) $g^{\varphi\varphi}(r^*)$ when $T^* = 2.20$ (dashed line) and when $T^* = 1.80$ (solid line).

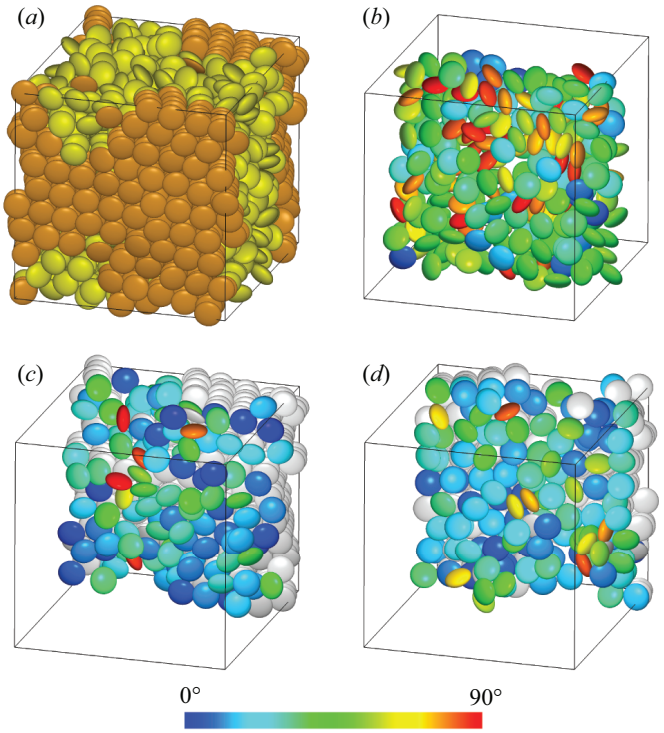

Fig. 15 Qualitative study on the liquid structure of Mixture III at the A-type/B-type liquid interface when $T^* = 2.20$. (*a*) Snapshot of the entire sample showing components by color, as in Fig. 6. (*b*) A liquid region away from the A-type/B-type interface, showing B-type discogens colored by molecular axis orientation. (*c*) A layer of B-type discogens (colored by molecular axis orientation) adjacent to the surface of A-type discogens (grayed out). (*d*) As in Panel (*c*), but for the anterior view (exposed by rotating the top face 180°). The color scheme for the orientation of molecular axes is given by the color scale (bottom).

The highly segregated state of Mixture III at nematic-like temperatures facilitates a qualitative study on the nature of the liquid structure at the A-type/B-type interface. Shown in Fig. 15 is a sample calculation when $T^* = 2.20$: the extent of phase segregation can be inferred from Fig. 15(*a*). In Figs. 15(*c*)-(*d*), A-type discogens have been grayed out, while B-type discogens are colored according to the orientation of individual molecular axes. The bulk-like region of B-type liquid (away from the interface) shows no preferred orientation [see Fig. 15(*b*)]. On the other hand, a layer of B-type liquid adjacent to A-type columnar "walls" [see Fig. 15(*c*) and Fig. 15(*d*)] displays induced liquid ordering (i.e., a higher proportion of B-type discogens displays hues of the same color). This study illustrates the orientational behavior of the A-type/B-type interface and underscores the inductive role that A-type discogens have in prompting the $C_{D,BB}$ phase.

3.3 Trends in Phase Behavior of the Binary Mixtures

In this section, the three mixtures investigated are considered collectively, summarizing important features and differences. To highlight specific trends, an analysis of the induced stabilization of the B-type columnar mesophase is provided in Table 3.

The figures of merit in Table 3 are now briefly defined. The temperatures where the first discontinuity is observed between the N_D and C_D phases for each component in the mixture are denoted $T^*_{AA,Col,mix}$ and $T^*_{BB,Col,mix}$. The change in temperature between $T^*_{AA,Col,mix}$ and the corresponding temperature for the pure liquid $T^*_{AA,Col}$ is given by $\Delta T^*_{AA} = T^*_{AA,Col,mix} - T^*_{AA,Col}$ (and analogously for the B component). Also listed in Table 3 is the value of $S(T^*)$ for the B component, $S_{BB}(T^*_{BB,Col,mix})$, as well as the difference between $S_{BB}(T^*_{BB,Col,mix})$ and the corresponding value of $S(T^*)$ for the A component, $S_{AA}(T^*_{BB,Col,mix})$, in the mixture (not shown in Table 3): that is, $\Delta S(T^*_{BB,Col,mix}) = S_{BB}(T^*_{BB,Col,mix}) - S_{AA}(T^*_{BB,Col,mix})$. These parameters are discussed in the context of the following points, which highlight salient features regarding the three mixtures treated in this work.

1. Thinner discogens form ordered phases more readily when compared to thicker discogens, as is evident in the strongly bidisperse sample (Mixture III): $S_{tot}(T^*)$ rises only gradually with cooling due to the prevailing disordered structure of the B component (though the A component already forms a columnar phase), between the $I_{L,BB}$ and $C_{D,BB}$ domains in Fig. 12. This effect arises because the *thicker* component has more rotational freedom due to a *higher* spherical resemblance than that of the *thinner* component. Thus, the B component requires cooler temperatures to maintain an ordered arrangement than does the A component.

2. The columnar mesophase for the B component is induced at higher temperatures (indicative of enhanced stability) in the presence of the A component. This stability is most pronounced for the weakly bidisperse sample (Mixture I): this conclusion is supported by comparing among the values of ΔT^*_{BB} in Table 3 for the three mixtures.

3. As the bidispersity index q increases (i.e., the difference in aspect ratio between discogen types decreases), the mixture is more stable against demixing. For example, consider the values of $T^*_{BB,Col,mix}$ in Table 3 together with Fig. 6. When cooling a strongly bidisperse sample (Mixture III), global segregation of disc types sets in and a range of temperatures emerges in which *paranematic*-like states appear. In

Table 3 Analysis of the induced stabilization of B-type columnar phases in the bidisperse mixtures.

Mixture	$T^*_{\mathrm{AA,Col,mix}}$	ΔT^*_{AA}	$T^*_{\mathrm{BB,Col,mix}}$	ΔT^*_{BB}	$S_{\mathrm{BB}}(T^*_{\mathrm{BB,Col,mix}})$	$\Delta S(T^*_{\mathrm{BB,Col,mix}})$
I	2.10 ± 0.02	-0.56	2.10 ± 0.02	$+0.42$	0.837 ± 0.009	-0.049
II	2.25 ± 0.02	-0.61	1.95 ± 0.02	$+0.27$	0.838 ± 0.009	-0.112
III	2.69 ± 0.02	-0.64	1.80 ± 0.02	$+0.12$	0.848 ± 0.008	-0.139

contrast, global segregation is not observed in the weakly bidisperse sample (Mixture I).

4. The columnar mesophase is induced in the weakly bidisperse sample (Mixture I) with the emergence of microheterogeneities. In turn, the columnar mesophase in the B component appears in the moderately and strongly bidisperse samples after there has been substantial fractionation between A and B components (e.g., see Fig. 6).

5. As the bidispersity index q decreases (i.e., discogen types become significantly different), the ability of the A component to induce a columnar mesophase is weakened due to a preemptive segregation of discogen types in the sample. This is manifested by an increasingly *gradual* response in $S_{\mathrm{BB}}(T^*)$ with cooling (e.g., compare Fig. 4 and Fig. 12).

6. The moderately bidisperse sample (Mixture II) presents a mixed pretransitional state, in which the A component experiences orientational frustration: B-type discogens hamper the formation of an otherwise ordered A-type mesophase. As a result, the sample exhibits several *prenematic*-like state points [i.e., a *gradual* increase in $S_{\mathrm{AA}}(T^*)$ *and* $S_{\mathrm{BB}}(T^*)$] before the mixture segregates to yield type-rich, orientationally-ordered phases. This behavior is analogous to the pretransitional effects observed in experimental measurements of discotic samples[64] and simulations of calamitic liquid crystals[86,167,168].

7. The strongly bidisperse sample (Mixture III) presents global phase segregation when temperatures are sufficiently low that $\mathrm{I_{L,AA}}$ is no longer stable. The *paranematic*-like ordering of B-type discogens occurs at the interface of A-type and B-type domains, for temperatures between the isotropic and nematic phases. The coexistence of an ordered layer of B-type discogens with an isotropic, bulk-like domain of the B component (away from the interface) produces a qualitatively distinct response in $S_{\mathrm{BB}}(T^*)$ (e.g., refer to Fig. 15).

8. Columnar mesophases appear to be stabilized by small aspect ratios (i.e., thin discogens) and strong orientation-dependent attractions. For instance, A-type discogens have a comparatively low aspect ratio ($\kappa_{\mathrm{AA}} = 0.286$) and a slightly strong attraction parameter ($\varepsilon_{0,\mathrm{AA}}/\varepsilon_{0,\mathrm{BB}} = 1.103$) in Mixture III [see Table 1 and Table 2]. This system yields the most negative value of $\Delta S(T^*_{\mathrm{BB,Col,mix}})$ [i.e., $S_{\mathrm{AA}}(T^*) > S_{\mathrm{BB}}(T^*)$] in Table 3. The other mixtures have less negative $\Delta S(T^*_{\mathrm{BB,Col,mix}})$ values as q increases (though $\varepsilon_{0,\mathrm{AA}}/\varepsilon_{0,\mathrm{BB}}$ also increases). The combined effect of geometry as well as attractions in A-type discogens enhances packing and prompts interdigitation in the $\mathrm{C_{D,AA}}$ phase (e.g., compare Fig. 11)[180].

4 Conclusions

Mixtures of DLCs provide an avenue to extend the appearance of useful mesophases and expand their range of application. In this work, binary equimolar mixtures of DLCs were treated. System bidispersity was introduced through molecular thickness, as opposed to mixtures of discoids with varying radii. This arrangement is weakly connected to experimental systems in which the molecular core is functionalized to promote "facial docking" as a means to enhance the stability of columnar mesophases, for instance, through a CPI paradigm. This work explored *weak*, *moderate*, and *strong* extents of bidispersity in molecular thickness. Results were contextualized to the interplay between orientational ordering transitions and system demixing as the bidispersity of the mixture changes.

In general, increasing the thickness bidispersity of discogens in a DLC mixture prompts demixing and leads to global phase segregation. When complete fractionation occurs, the system behaves as two independent ordered domains. This orientation independence manifests itself as two coexisting bulk-like phases, each yielding a characteristic order parameter consistent with the state point of the mixture. However, a striking feature is that liquid orientation can be "communicated" to an adjacent liquid layer to yield, for instance, a *paranematic*-like structure. This interface-induced phenomenon occurs in a way that the highly-oriented liquid (i.e., the thin discogen) "transfers" order to the less-oriented liquid (i.e., the thick discogen). This produces an earlier (but sluggish) onset of the columnar mesophase for the less-oriented liquid as orientational order permeates through the disordered, bulk-like domain. A variant of this mechanism is observed in the moderately bidisperse system, in which the sample remains mixed, giving rise to orientational frustration that results in *prenematic*-like state points. These mechanisms effectively widen the temperature range for experimentally-relevant DLC mesophases.

For the weakly bidisperse mixture, orientational order permeates the sample without having to undergo global segregation. The onset of the columnar mesophase is observed at higher (i.e., destabilizing) temperatures. When considering the three cases of bidispersity, a design principle concerning the stability of mixtures emerges: increasing the extent of bidispersity (i.e., decreasing the bidispersity parameter q) destabilizes mixture homogeneity. In an applied sense, the onset of the columnar mesophase is favored in mixtures with small bidispersity and broadens the working range of columnar samples toward higher temperatures. Lacking a theoretical construct for making quantitative predictions, it is supposed that there exists a critical value of q that optimizes a balance between the induction of columnar phases and sample demixing.

When considering moderately and strongly bidisperse mix-

tures, two distinct mechanisms can be identified in the induction of columnar mesophases. In the case of the moderately bidisperse mixture, a pretransitional effect emerges: from an initially isotropic state, a mixed *prenematic*-like phase causes the sample to undergo greater orientational order with cooling (smoothly and gradually, as detected by the orientational order parameter). This eventually yields a segregated nematic phase in the mixture, which then turns into a segregated columnar arrangement upon further cooling. The loss of a discontinuous I_L-N_D transition originates from the orientational frustration that A-type discogens experience: well-posed to form an ordered liquid phase, A-type discogens cannot do so globally due to the presence of surrounding B-type discogens. On the other hand, A-type discogens stabilize orientational fluctuations of the more disordered B-type discogens, so that a mixed *prenematic*-like phase is observed.

A less efficient induction of the columnar phase is seen in the strongly bidisperse mixture. Samples of the mixture readily segregate into two bulk-like domains, each consisting mostly of one component. There is only an I_L-C_D transition [detected by a discontinuity in $S(T^*)$] for the A-type fluid. The B-type fluid smoothly and gradually forms the columnar phase upon cooling: there is no evident discontinuity in $S(T^*)$. Specifically, the B-type fluid reaches $S(T^*)$ values for the N_D phase by a mechanism similar to that driving *paranematic*-like samples: B-type fluid adjacent to the highly-ordered A-type columnar phase is more structured than the bulk-like region of the B component. This induced order gradually permeates the sample upon further cooling to yield the $C_{D,BB}$ phase for a slightly earlier (higher) T^*, and less efficiently so when compared to weakly or moderately bidisperse mixtures.

The *paranematic*-like effect in the strongly bidisperse mixture is not due to confinement or an external field, as seen in other liquid-crystalline systems. Instead, the induced order in the B-type discogen is due to fluid layering against the A-type columnar phase: this interfacial effect is peculiar to the strongly bidisperse mixture. Our study on fluid layering (see Fig. 15) cautions against reporting order parameter averages without accounting for a distinctly-ordered domain of another component in the mixture [e.g., through a strong oscillatory response in type-resolved orientational order parameters that probe along a spatial axis, such as $S(r_\gamma)$]. Our conclusions are somewhat limited in that sample dimensions for other cases may give rise to behavioral discrepancies in $S(T^*)$. For example, a system that masks the interfacial contribution by favoring a bulk-like domain may alter the approximate T^{-1} dependence of the B-type response in $S(T^*)$. However, the interfacial contribution will be present regardless of system size. The complex phase behavior of the strongly bidisperse mixture reveals an important variant for inducing orientational arrangements when homogeneous mixtures are not viable.

An important extension of our findings is the phase behavior of DLC mixtures handled at lower pressures (i.e., our studies focused on a relatively high pressure of $P^* = 25.0$). A study based on changing the system pressure can reveal other aspects of how mixture concentration couples with sample bidispersity. Along a related vein, a study in which bidispersity is introduced with respect to radial dimension (i.e., core size) can extend our understanding of how coexisting molecular types prompt phase segregation and produce variants in columnar packing. An issue of interest for charge-transport applications is identifying the extent to which discogen types stably alternate along a columnar axis or form microsegregated domains. Moreover, a relevant study is to test how well the Gay-Berne model captures the requisite phenomenology, in light of its coarse-grained nature. Once a static description has been established for mixtures, a subsequent natural step is to perform analyses related to system dynamics. For instance, being able to relate mixture bidispersity with diffusivity could aid in outlining stability conditions against segregation for specific mesophases and guide the design of molecules that promote mixture homogeneity or drive phase segregation. Some of these questions are already being pursued by our group. The goal is to attain a more complete molecular picture that relates to the phenomenology of DLC mixtures, especially with regard to the contributions that lead to self-organization modes, stability conditions, and material responses useful in applied technologies.

5 Acknowledgments

We gratefully acknowledge the financial support provided by CONACYT-Mexico (Project No. 178963). O. C.-C. and C. G.-A. thank CONACYT-Mexico for a graduate and a postdoctoral scholarship, respectively. J. A. M.-R., E. D.-H., and E. J. S. acknowledge an International Travel Grant Award from the American Physical Society. J. A. M.-R. is grateful to DGTIC-UNAM (Project No. SC14-1-I-60) for computing time. Additional computing resources were provided by LSVP at UAM-I and the Xiuhcoatl Supercomputing Hybrid Cluster at CINVESTAV (Mexico).

Notes and references

1 S. Kumar, *Chemistry of Discotic Liquid Crystals: From Monomers to Polymers*, CRC Press, Boca Raton, FL, 2011, pp. 18–28.

2 Other discotic systems have been synthesized without having to employ a polycyclic core from the outset. In this case, a discoid template results from the self-organization of simpler molecular units (often non-mesogenic) that yields a discogenic template [181–191].

3 H. K. Bisoyi and S. Kumar, *Chem. Soc. Rev.*, 2011, **40**, 306–319.

4 P. G. de Gennes and J. Prost, *The Physics of Liquid Crystals*, Claredon Press, Oxford, 2 edn, 1993.

5 C. Xue, S. Jin, X. Weng, J. J. Ge, Z. Shen, H. Shen, M. J. Graham, K.-U. Jeong, H. Huang, D. Zhang, M. Guo, F. W. Harris, S. Z. D. Cheng, C. Y. Li and L. Zhu, *Chem. Mater.*, 2004, **16**, 1014–1025.

6 S. Chandrasekhar, *Liq. Cryst.*, 1993, **14**, 3–14.

7 S. Chandrasekhar, *Mol. Cryst. Liq. Cryst.*, 1981, **63**, 171–179.

8 J. Barberá, C. Cativiela, J. L. Serrano and M. M. Zurbano, *Adv. Mater.*, 1991, **3**, 602–605.

9 H. Shen, K.-U. Jeong, H. Xiong, M. J. Graham, S. Leng, J. X. Zheng, H. Huang, M. Guo, F. W. Harris and S. Z. D. Cheng, *Soft Matter*, 2006, **2**, 232–242.

10 R. J. Bushby and O. R. Lozman, *Curr. Op. Coll. and Int. Sci.*, 2002, **7**, 343–354.

11 H. Zhang, C. K. Lai and T. Swager, *Chem. Mater.*, 1995, **7**, 2067–2077.

12 S. Jin, Y. Ma, S. C. Zimmerman and S. Z. D. Cheng, *Chem. Mater.*, 2004, **16**, 2975–2977.

13 C. Piechocki, J. Simon, A. Skoulios, D. Guillon and P. Weber, *J. Am. Chem. Soc.*, 1982, **104**, 5245–5247.

14 H. Shen, K.-U. Jeong, M. J. Graham, S. Leng, H. Huang, B. Lotz, H. Hou, F. W. Harris and S. Z. D. Cheng, *J. Macrom. Sci. Part B: Phys.*, 2006, **45**, 215–229.

15 C. Pugh and V. Percec, *J. Mater. Chem.*, 1991, **1**, 765–773.

16 F. Ciuchi, G. D. Nicola, H. Franz, G. Gottarelli, P. Mariani, M. G. P. Bossi and G. P. Spada, *J. Am. Chem. Soc.*, 1994, **116**, 7064–7071.

17 G. Ungar, D. Abramic, V. Percec and J. A. Heck, *Liq. Cryst.*, 1996, **21**, 73–86.

18 H. Bock and W. Helfrich, *Liq. Cryst.*, 1992, **12**, 697–703.

19 H. Bock and W. Helfrich, *Liq. Cryst.*, 1995, **18**, 387–399.

20 J. Simmerer, B. Glusen, W. P. A. Kettner, P. Schuhmacher, D. Adam, K. Etzbach, K. Siemensmeyer, J. H. Wendorff, H. Ringsdorf and D. Haarer, *Adv. Mater.*, 1996, **8**, 815–819.

21 D. Adam, F. Closs, T. Frey, D. Funhoff, D. Haarer, H. Ringsdorf, P. Schuhmacher and K. Siemensmeyer, *Phys. Rev. Lett.*, 1993, **70**, 457–460.

22 F. Closs, K. Siemensmeyer, T. Frey and D. Funho, *Liq. Cryst.*, 1993, **14**, 629–634.

23 D. Adam, P. Schuhmacher, J. Simmerer, L. Häussling, K. Siemensmeyer, K. H. Etzbacj, H. Ringsdorf and D. Haarer, *Nature*, 1994, **371**, 141–143.

24 H. Bengs, F. Closs, T. F. D. Funhoff, H. Ringsdorf and K. Siemensmeyer, *Liq. Cryst.*, 1993, **15**, 565–574.

25 G. B. M. Vaughan, P. A. Heiney, J. P. McCauley Jr. and A. B. Smith III, *Phys. Rev. B*, 1992, **46**, 2787–2791.

26 N. Boden, R. J. Bushby and J. Clements, *J. Chem. Phys.*, 1993, **98**, 5920–5931.

27 T. Matsui, T. Nagata, M. Ozaki, A. Fujii, M. Onoda, M. Teraguchi, T. Masuda and K. Yoshino, *Synth. Met.*, 2001, **119**, 599–600.

28 E. O. Arikainen, N. Boden, R. J. Bushby, J. Clements, B. Movaghar and A. Wood, *J. Mater. Chem.*, 1995, **5**, 2161–2165.

29 A. M. van de Craats and J. M. Warman, *Adv. Mater.*, 2001, **13**, 130–133.

30 S. Kumar, *Chem. Soc. Rev.*, 2006, **35**, 83–109.

31 S. Kumar, *Liq. Cryst.*, 2009, **36**, 607–638.

32 D. Demus, *Mol. Cryst. Liq. Cryst.*, 2001, **364**, 25–91.

33 C. D. Simpson, J. Wu, M. D. Watson and K. Müllen, *J. Mater. Chem.*, 2004, **14**, 494–504.

34 T. Hassheider, S. A. Benning, M. W. Lauhof, R. Oesterhaus, S. Alibert-Fouet, H. Bock, J. W. Goodby, M. D. Watson, K. Müllen and H.-S. Kitzerow, Proceedings of SPIE-IS&T, 2003, pp. 167–174.

35 W. Pisula, A. Menon, M. Stepputat, I. Lieberwirth, U. Kolb, A. Tracz, H. Sirringhaus, T. Pakula and K. Müllen, *Adv. Mater.*, 2005, **17**, 684–689.

36 J. W. Goodby, I. M. Saez, S. J. Cowling, V. Görtz, M. Draper, A. W. Hall, S. Sia, G. Cosquer, S.-E. Lee and E. P. Raynes, *Angew. Chem. Int. Ed.*, 2008, **47**, 2754–2787.

37 J. W. Goodby, I. M. Saez, S. J. Cowling, J. S. Gasowska, R. A. MacDonald, S. Sia, P. Watson, K. J. Toyne, M. Hird, R. A. Lewis, S.-E. Lee and V. Vaschenko, *Liq. Cryst.*, 2009, **36**, 567–605.

38 K. Kawata, *Chem. Rec.*, 2002, **2**, 59–80.

39 H. K. Bisoyi and S. Kumar, *Chem. Soc. Rev.*, 2010, **39**, 264–285.

40 J. J. Ge, S. C. Hong, B. Y. Tang, C. Y. Li, D. Zhang, T. Bai, B. Mansdorf, F. W. Harris, D. Yang, Y. R. Shen and S. Z. D. Cheng, *Adv. Func. Mater.*, 2003, **13**, 718–725.

41 H. Mori, Y. Itoh, Y. Nishiura, T. Nakamura and Y. Shinagawa, *Jpn. J. Appl. Phys.*, 1997, **36**, 143–147.

42 H. Mori, *J. Disp. Technol.*, 2005, **1**, 179–186.

43 S. Müller and K. Müllen, *Phil. Trans. R. Soc. A*, 2007, **365**, 1453–1472.

44 S. Sergeyev, W. Pisula and Y. H. Geerts, *Chem. Soc. Rev.*, 2007, **36**, 1902–1929.

45 V. Duzhko, H. Shi, K. D. Singer, A. N. Semyonov and R. J. Twieg, *Langmuir*, 2006, **22**, 7949–7951.

46 S. Xiao, M. Myers, Q. Miao, S. Sanaur, K. Pang, M. L. Steigerwald and C. Nuckolls, *Angew. Chem. Int. Ed.*, 2005, **44**, 7390–7394.

47 Z. H. Al-Lawati, B. Alkhairalla, J. P. Bramble, J. R. Henderson, R. J. Bushby and S. D. Evans, *J. Phys. Chem.*, 2012, **116**, 12627–12635.

48 J. Wu, W. Pisula and K. Müllen, *Chem. Rev.*, 2007, **107**, 718–747.

49 C. Tschierske, *Angew. Chem. Int. Ed.*, 2013, **52**, 8828–8878.

50 R. J. Bushby, K. J. Donovan, T. Kreouzis and O. R. Lozman, *Opto-Electron. Rev.*, 2005, **13**, 269–279.

51 K. Praefcke, D. Singer, M. Langner, B. Kohne, M. Ebert, A. Liebmann and J. H. Wendorff, *Mol. Cryst. Liq. Cryst.*, 1992, **215**, 121–126.

52 D. Janietz and A. Kohlmeier, *Liq. Cryst.*, 2009, **36**, 685–703.

53 O. R. Lozman, R. J. Bushby and J. G. Vinter, *J. Chem. Soc., Perkin Trans. 2*, 2001, 1446–1452.

54 N. Boden, R. J. Bushby, Q. Liu and O. R. Lozman, *J. Mater. Chem.*, 2001, **11**, 1612–1617.

55 N. Boden, R. J. Bushby, G. Cooke, O. R. Lozman and Z. Lu, *J. Am. Chem. Soc.*, 2001, **123**, 7915–7916.

56 E. O. Arikainen, N. Boden, R. J. Bushby, O. R. Lozman, J. G. Vinter and A. Wood, *Angew. Chem. Int. Ed.*, 2000, **39**, 2333–2336.

57 C. A. Hunter and J. K. M. Sanders, *J. Am. Chem. Soc.*, 1990, **112**, 5525–5534.

58 C. A. Hunter, *Angew. Chem. Int. Ed.*, 1993, **32**, 1584–1586.

59 J. G. Vinter, *J. Comput.-Aided Mol. Des.*, 1994, **8**, 653–668.

60 T. Kreouzis, K. Scott, K. J. Donovan, N. Boden, R. J. Bushby, O. R. Lozman and Q. Liu, *Chem. Phys.*, 2000, **262**, 489–497.

61 C. Destrade, N. H. Tinh, J. Malthete and J. Jacques, *Phys. Lett. A*, 1980, **79**, 189–192.

62 S. Chandrasekhar, C. Frank, J. D. Litster, W. H. D. Jeu and L. Lei, *Philos. Trans. R. Soc. London, Ser. A*, 1983, **309**, 93–103.

63 J. Billard and B. Sadashiva, *Pramana*, 1979, **13**, 309–318.

64 C. Baumann, J. P. Marcerou, J. C. Jouillon and J. Prost, *J. Phys. (Paris)*, 1984, **45**, 451–458.

65 C. Destrade, P. Foucher, H. Gasparoux, N. H. Tinh, A. M. Levelut and J. Malthete, *Mol. Cryst. Liq. Cryst.*, 1984, **106**, 121–146.

66 E. Fontes, P. A. Heiney, M. Ohba, J. N. Haseltine and A. B. Smith III, *Phys. Rev. A*, 1988, **37**, 1329–1334.

67 C. Destrade, N. H. Tinh, H. Gasparoux, J. Malthete and A. M. Levelut, *Mol. Cryst. and Liq. Cryst.*, 1981, **71**, 111–135.

68 C. Destrade, M. C. Mondon-Bernaud and N. H. Tinh, *Mol. Cryst. and Liq. Cryst.*, 1979, **49**, 169–174.

69 C. Destrade, H. Gasparoux, P. Foucher, N. H. Tinh, J. Malthete and J. Jacques, *J. Chim. Phys.*, 1983, **80**, 137–148.

70 C. Destrade, N. H. Tinh, J. Malthete and A. M. Levelut, *J. Phys. (Paris)*, 1983, **44**, 597–602.

71 C. Destrade, J. Malthete, N. H. Tinh and H. Gasparoux, *Phys. Lett. A*, 1980, **78**, 82–84.

72 T. Warmerdam, D. Frenkel and R. J. J. Zijlstra, *Liq. Cryst.*, 1998, **3**, 149–152.

73 W. K. Lee, B. A. Wintner, E. Fontes, P. A. Heiney, M. Ohba, J. N. Haseltine and A. B. Smith III, *Liq. Cryst.*, 1989, **4**, 87–102.

74 V. Percec, J. Heck, G. Johansson, D. Tomazos, M. Kawasumi, P. Chu and G. Ungar, *Mol. Cryst. Liq. Cryst.*, 1994, **254**, 137–196.

75 V. Percec, M. Lee, J. Heck, H. E. Blackwell, G. Ungar and A. Alvarez-Castillo, *J. Mater. Chem.*, 1992, **2**, 931–938.

76 C. Destrade, H. Gasparoux, A. Babeau, N. H. Tinh and J. Malthete, *Mol. Cryst. Liq. Cryst.*, 1981, **67**, 37–47.

77 C. Destrade, P. Foucher, J. Malthete and N. H. Tinh, *Phys. Lett. A*, 1982, **88**, 187–190.

78 N. H. Tinh, J. Malthête and C. Destrade, *J. Physique Lett.*, 1981, **42**, 417–419.

79 N. H. Tinh, J. Malthete and C. Destrade, *Mol. Cryst. Liq. Cryst.*, 1981, **64**, 291–298.

80 N. H. Tinh, P. Foucher, C. Destrade, A. M. Levelut and J. Malthete, *Mol. Cryst. Liq. Cryst.*, 1984, **111**, 277–292.

81 M. G. Mazza and M. Schoen, *Int. J. Mol. Sci.*, 2011, **12**, 5352–5372.

82 J. Szydłowska, A. Krówczyński, R. Bilewicz, D. Pociecha and Ł. Głaz, *J. Mater. Chem.*, 2008, **18**, 1108–1115.

83 S. Singh, *Phys. Rep.*, 2000, **324**, 107–269.

84 H. Bengs, M. Ebert, O. Karthaus, B. Kohne, K. Praefcke, H. Ringsdorf, J. H. Wendorff and R. Wüstefeld, *Adv. Mater.*, 1990, **2**, 141–144.

85 K. Praefcke, D. Singer, B. Kohne, M. Ebert, A. Liebmann and J. H. Wendorff, *Liq. Cryst.*, 1991, **10**, 147–159.

86 J. A. Moreno-Razo, E. Díaz-Herrera and S. H. L. Klapp, *Phys. Rev. E*, 2007, **76**, 041703.

87 C. Park, H. J. Song and H. C. Choi, *Chem. Commun.*, 2009, 4803–4805.

88 S. Lee, S. Oh, S. Lee, Y. Malpani, Y.-S. Jung, B. Kang, J. Y. Lee, K. Ozasa, T. Isoshima, S. Y. Lee, M. Hara, D. Hashizume and J.-M. Kim, *Langmuir*, 2013, **29**, 5869–5877.

89 I. Cour, Z. Pan, L. T. Lebruin, M. A. Case, M. Furis and R. L. Headrick, *Org. Electron.*, 2012, **13**, 419–424.

90 R. J. Gupta, V. Manjuladevi, C. Karthik and S. Kumar, *J. Phys.: Conf. Ser.*, 2013, **417**, 012068.

91 R. K. Gupta, V. Manjuladevi, C. Karthik, S. Kumar and K. A. Suresh, *Colloids and Surfaces A: Physicochemical and Engineering Aspects*, 2012, **410**, 91–97.

92 R. K. Gupta and V. Manjuladevi, *Isr. J. Chem.*, 2012, **52**, 809–819.

93 C. Karthik, V. Manjuladevi, R. K. Gupta and S. Kumar, *J. Mol. Struct.*, 2014, **1070**, 52–57.

94 A. Albrecht, W. Cumming, W. Kreuder, A. Laschewsky and H. Ringsdorf, *Col. Polym. Sci.*, 1986, **264**, 659–667.

95 D. Gidalevitz, O. Y. Mindyuk, P. A. Heiney, B. M. Ocko, P. Henderson, H. Ringsdorf, N. Boden, R. J. Bushby, P. S. Martin, J. Strzalka, J. P. McCauley Jr. and A. B. Smith III, *J. Phys. Chem. B*, 1997, **101**, 10870–10875.

96 N. C. Maliszewskyj, P. A. Heiney, J. K. Blasie, J. P. McCauley Jr. and A. B. Smith III, *J. Phys. II (France)*, 1992, **2**, 75–85.

97 N. C. Maliszewskyj, P. A. Heiney, J. Y. Josefowicz, J. P. McCauley Jr. and A. B. Smith III, *Science*, 1994, **264**, 77–79.

98 N. C. Maliszewskyj, O. Y. Mindyuk, P. A. Heiney, J. Y. Josefowicz, P. Schuhmacher and H. Ringsdorf, *Liq. Cryst.*, 1999, **26**, 31–36.

99 A. Nayak, K. A. Suresh, S. K. Pal and S. Kumar, *J. Phys. Chem. B*, 2007, **111**, 11157–11161.

100 D. W. Breiby, F. Hansteen, W. Pisula, O. Bunk, U. Kolb, J. W. Andreasen, K. Müllen and M. M. Nielsen, *J. Phys. Chem. B*, 2005, **109**, 22319–22325.

101 G. Gbabode, N. Dumont, F. Quist, G. Schweicher, A. Moser, P. Viville, R. Lazzaroni and Y. H. Geerts, *Adv. Mater.*, 2012, **24**, 658–662.

102 E. Charlet, E. Grelet, P. Brettes, H. Bock, H. Saadaoui, L. Cisse, P. Destruel, N. Gheradi and I. Seguy, *Appl. Phys. Lett.*, 2008, **92**, 024107.

103 V. D. Cupere, J. Tant, P. Viville, R. Lazzaroni, W. Osikowic, W. R. Salaneck and Y. H. Geerts, *Langmuir*, 2006, **22**, 7798–7806.

104 A. Calo, P. Stoliar, M. Cavallini, S. Sergeyev, Y. H. Geerts and F. Biscarini, *J. Am. Chem. Soc.*, 2008, **130**, 11953–11958.

105 P.-O. Mouthuy, S. Melinte, Y. H. Geerts and A. M. Jonas, *Nano Lett.*, 2007, **7**, 2627–2632.

106 E. Grelet, S. Dardel, H. Bock, M. Goldmann, E. Lacaze and F. Nallet, *Eur. Phys. J. E*, 2010, **31**, 343–349.

107 Z. Shen, M. Yamada and M. Miyake, *J. Am. Chem. Soc.*, 2007, **129**, 14271–14280.

108 M. Yamada, Z. Shen and M. Miyake, *Chem Commun.*, 2006, 2569–2571.

109 B. S. Avinash, V. Lakshminarayanan, S. Kumar and J. K. Vij, *Chem. Commun.*, 2013, 978–980.

110 Supreet, S. Kumar, K. K. Raina and R. Pratibha, *Liq. Cryst.*, 2013, **4**, 228–236.

111 S. Kumar, S. K. Pal, P. S. Kumar and V. Lakshminarayanan, *Soft Matter*, 2007, **3**, 896–900.

112 S. Kumar and H. K. Bisoyi, *Angew. Chem. Int. Ed.*, 2007, **46**, 1501–1503.

113 P. S. Kumar, S. K. Pal, S. Kumar and V. Lakshminarayanan, *Langmuir*, 2007, **23**, 3445–3449.

114 S. Kumar and L. K. Sagar, *Chem. Commun.*, 2011, **47**, 12182–12184.

115 L. Y. Chiang, J. P. Stokes, C. R. Safinya and A. N. Bloch, *Mol. Cryst. Liq. Cryst.*, 1985, **125**, 279–288.

116 J. van Keulen, T. W. Warmerdam, R. J. M. Nolte and W. Drenth, *Recl. Trav. Chim. Pays-Bas.*, 1987, **106**, 534–536.

117 V. S. K. Balagurusamy, S. K. Prasad, S. Chandrasekhar, S. Kumar, M. Manickam and C. V. Yelamaggad, *Pramana*, 1999, **53**, 3–11.

118 H. K. Bisoyi and S. Kumar, *J. Mater. Chem.*, 2008, **18**, 3032–3039.

119 S. Chandrasekhar and V. S. K. Balagurusamy, *Proc. R. Soc. Lond. A*, 2002, **458**, 1783–1794.

120 D. Vijayaraghavan and S. Kumar, *Mol. Cryst. Liq. Cryst.*, 2009, **508**, 101–114.

121 S. Kumar and V. Lakshminarayanan, *Chem. Commun.*, 2004, 1600–1601.

122 P. S. Kumar, S. Kumar and V. Lakshminarayanan, *J. Phys. Chem. B*, 2008, **112**, 4865–4869.

123 S. Kumar, *Liq. Cryst.*, 2014, **41**, 353–367.

124 N. Boden, R. J. Bushby, G. Headdock, O. R. Lozman and A. Wood, *Liq. Cryst.*, 2001, **28**, 139–144.

125 T. Kreouzis, K. J. Donovan, N. Boden, R. J. Bushby, O. R. Lozman and Q. Liu, *J. Chem. Phys.*, 2001, **114**, 1797–1802.

126 N. Boden and B. Movaghar, in *Applicable Properties of Columnar Discotic Liquid Crystals*, ed. D. Demus, J. Goodby, G. W. Gray, H.-W. Spiess and V. Vill, Wiley, Weinheim, 1998, vol. 2B, pp. 782–798.

127 N. Boden, R. J. Bushby, J. Clements and B. Movaghar, *J. Chem. Mater.*, 1999, **9**, 2081–2086.

128 W. Pisula, M. Kastler, D. Wasserfallen, J. W. F. Robertson, F. Nolde, C. Kohl and K. Müllen, *Angew. Chem. Int. Ed.*, 2006, **45**, 819–823.

129 B. R. Wegewijs and L. D. A. Siebbeles, *Phys. Rev. B*, 2002, **65**, 245112.

130 T. Coussaert and M. Baus, *J. Chem. Phys.*, 2002, **116**, 7744–7751.

131 D. de las Heras and M. Schmidt, *Phil. Trans. R. Soc. A.*, 2013, **371**, 20120259.

132 A. Galindo, G. Jackson and D. J. Photinos, *Chem. Phys. Lett.*, 2000, **325**, 631–638.

133 A. Galindo, A. J. Haslam, S. Varga, G. Jackson, A. G. Vanakaras, D. J. Photinos and D. A. Dunmur, *J. Chem. Phys.*, 2003, **119**, 5216–5225.

134 F. Gamez, R. D. Acemel and A. Cuetos, *Mol. Phys.*, 2013, **111**, 3136–3146.

135 J. Landman, E. Paineau, P. Davidson, I. Bihannic, L. J. Michot, A.-M. Philippe, A. V. Petukhov and H. N. W. Lekkerkerker, *J. Phys. Chem. B*, 2014, **118**, 4913–4919.

136 M. Chen, H. Li, Y. Chen, A. F. Mejia, X. Wang and Z. Cheng, *Soft Matter*, 2015, **11**, 5775–5779.

137 N. Doshi, G. Cinacchi, J. S. van Duijneveldt, T. Cosgrove, S. W. Prescott, I. Grillo, J. Phipps and D. I. Gittins, *J. Phys.: Condens. Matter*, 2011, **23**, 194109.

138 J. Phillips and M. Schmidt, *Phys. Rev. E*, 2010, **81**, 041401.

139 H. N. W. Lekkerkerker, R. Tuinier and H. H. Wensink, *Mol. Phys.*, 2015, **Special Issue in Honour of Jean-Pierre Hansen**, 1–8.

140 T. Nakato, Y. Yamashita, E. Mouri and K. Kuroda, *Soft Matter*, 2014, **10**, 3161–3165.

141 M. Golmohammadi and A. D. Rey, *Entropy*, 2008, **10**, 183–199.

142 M. Golmohammadi and A. D. Rey, *Liq. Cryst.*, 2009, **36**, 75–92.

143 G. Cinacchi and A. Tani, *J. Chem. Phys.*, 2002, **117**, 11388–11395.

144 M. A. Bates and G. R. Luckhurst, *Liq. Cryst.*, 1998, **24**, 229–241.

145 M. A. Bates, *Liq. Cryst.*, 2003, **30**, 181–190.

146 J. Idé, R. Méreau, L. Ducasse, F. Castet, H. Bock, Y. Olivier, J. Cornil, D. Beljonne, G. D'Avino, O. M. Roscioni, L. Muccioli and C. Zannoni, *J. Am. Chem. Soc.*, 2014, **136**, 2911–2920.

147 O. Cienega-Cacerez, J. A. Moreno-Razo, E. Díaz-Herrera and E. J. Sambriski, *Soft Matter*, 2014, **10**, 3171–3182.

148 D. J. Cleaver, C. M. Care, M. P. Allen and M. P. Neal, *Phys. Rev. E*, 1996, **54**, 559–567.

149 J. G. Gay and B. J. Berne, *J. Chem. Phys.*, 1981, **74**, 3316–3319.

150 M. A. Bates and G. R. Luckhurst, *J. Chem. Phys.*, 1996, **104**, 6696–6709.

151 M. A. Bates and G. R. Luckhurst, *J. Chem. Phys.*, 1999, **110**, 7087–7108.

152 D. Caprion, L. Bellier-Castella and J. P. Ryckaert, *Phys. Rev. E.*, 2003, **67**, 041703.

153 A. P. J. Emerson, G. R. Luckhurst and S. G. Whatling, *Mol. Phys.*, 1994, **82**, 113–124.

154 J. M. Ilnytskyi and M. R. Wilson, *Comp. Phys. Comm.*, 2001, **134**, 23–32.

155 J. M. Ilnytskyi and M. R. Wilson, *Comp. Phys. Comm.*, 2002, **148**, 43–58.

156 T. Gruhn and M. Schoen, *Phys. Rev. E*, 1997, **55**, 2861–2875.

157 K. Singer, A. Taylor and J. V. L. Singer, *Mol. Phys.*, 1977, **33**, 1757–1795.

158 J. Billeter and R. Pelcovits, *Comput. Phys.*, 1998, **12**, 440–448.

159 In a body-fixed frame, three non-vanishing contributions to the moment of inertia apply to the discogen: two identical contributions *perpendicular* to the principal axis [$I_{\perp,aa} = (1/20)\, m_{aa}\, \sigma_{0,aa}{}^2 \left(\kappa_{aa}{}^2 + 1\right)$] and one distinct contribution *parallel* to the principal axis [$I_{\parallel,aa} = (1/10)\, m_{aa}\, \sigma_{0,aa}{}^2$]. A

technical matter is that $I_{\parallel,aa}$ cannot be efficiently accounted for in a model for which the discogen is represented by a center-of-mass site (i.e., the orientation of the discogen is unknown within the molecular plane). In practice, the equations of rotational motion can be taken into account with a single, non-zero (though somewhat arbitrary) scalar based on a quaternion formalism. In effect, it is possible to describe the orientational evolution of the molecular principal axis with time using this approach [158]. For simplicity, the scalar in the quaternion approach was set to $I_{\perp,aa}$.

160 M. P. Allen and D. J. Tildesley, *Computer Simulations of Liquids*, Clarendon Press, Oxford, 1987, pp. 304–306.

161 J.-P. Hansen and I. R. McDonald, *Theory of Simple Liquids with Applications to Soft Matter*, Academic Press, Oxford, 4 edn, 2013, p. 110.

162 The scheme used to designate discotic mesophases is as follows: I_G = isotropic gas phase; I_L = isotropic liquid phase; N_D = discotic nematic phase; C_O = ordered columnar (rectangular) phase; C_D = disordered columnar (hexagonal) phase. This nomenclature is consistent with our previous work on a Gay-Berne discotic system [147].

163 The values of P^* referenced for the C_D and C_O phases result in an interval that was not studied due to limited computational time. The crossover from the C_D phase to the C_O phase occurs at $6.0 < P^* < 8.0$ for the *thin* discogen and at $12.5 < P^* < 16.5$ for the *thick* discogen. To visualize the associated intervals on the corresponding phase diagrams, see the regions highlighted with arrows in Fig. 2.

164 A "true" nematic (N_D) phase can be appreciated in Fig. 4(*a*) of our previous work on a triphenylene-core discotic system [147] (which corresponds to the orientational behavior observed for a pure liquid). Here, the *paranematic*-like (*para*-N_D) phase is shown due to its importance when dealing with discotic mixtures, as discussed subsequently for a *strongly* bidisperse mixture.

165 A. T. Gabriel, T. Meyer and G. Germano, *J. Chem. Theory Comput.*, 2008, **4**, 468–476.

166 In analogy with the designations given to type-resolved order parameters $S_{aa}(T^*)$ for pure liquids and mixtures [e.g., $S_{AA}(T^*)$ and $S_{AA}{}'(T^*)$], a similar scheme is used to specify orientational phases of disc types. For instance, when comparing the columnar phase (C_D) of the A-type discogen, the designation $C_{D,AA}$ and $C_{D,AA}{}'$ is used, respectively.

167 R. A. Bemrose, C. M. Care, D. J. Cleaver and M. P. Neal, *Mol. Cryst. Liq. Cryst.*, 1997, **299**, 27–32.

168 R. A. Bemrose, C. M. Care, D. J. Cleaver and M. P. Neal, *Mol. Phys.*, 1997, **90**, 625–635.

169 R. Berardi, S. Orlandi and C. Zannoni, *Liq. Cryst.*, 2005, **32**, 1427–1436.

170 J. A. Moreno-Razo, E. J. Sambriski, G. M. Koenig, E. Díaz-Herrera, N. L. Abbott and J. J. de Pablo, *Soft Matter*, 2011, **7**, 6828–6835.

171 J. K. Whitmer, A. A. Joshi, T. F. Roberts and J. J. de Pablo, *J. Chem. Phys.*, 2013, **138**, 194903.

172 S. J. Mills, C. M. Care, M. P. Neal and D. J. Cleaver, *Phys. Rev. E*, 1998, **58**, 3284–3294.

173 A. V. Kityk, M. Wolff, K. Knorr, D. Morineau, R. Lefort and P. Huber, *Phys. Rev. Lett.*, 2008, **101**, 187801.

174 E. Cañeda-Guzmán, J. A. Moreno-Razo, E. Díaz-Herrera and E. J. Sambriski, *Mol. Phys.*, 2014, **112**, 1149–1159.

175 S. Całus, B. Jabłońska, M. Busch, D. Rau, P. Huber and A. Kityk, *Phys. Rev. E*, 2014, **89**, 062501.

176 Z. Lin, H. Zhang and Y. Yang, *Phys. Rev. E*, 1998, **58**, 5867–5872.

177 X. Zhou, H. Chen and M. Iwamoto, *J. Chem. Phys.*, 2004, **120**, 1832–1836.

178 W. H. de Jeu, L. Longa and D. Demus, *J. Chem. Phys.*, 1986, **84**, 6410–6420.

179 J. C. Hwang, S. C. Lang, K. H. Liang and J. R. Chang, *Liq. Cryst.*, 1999, **26**, 925–930.

180 Interdigitation in columnar mesophases has been previously observed for a triphenylene-like discogen model, in both hexagonal [147,152] and rectangular [147] packing of columns. The oblate hard spherocylinder (OHSC) model of disc-like geometry also displays interdigitation [192–194]. This suggests that interdigitation is not exclusive of Gay-Berne discogens, but rather an effect driven by packing through molecular geometry and attractive interactions [192,193].

181 J. H. Lee, I. Jang, S. H. Hwang, S. J. Lee, S. H. Yoo and J. Y. Jho, *Liq. Cryst.*, 2012, **39**, 973–981.

182 F. Sander, S. Tussetschläger, S. Sauer, M. Kaller, K. V. Axenov and S. Laschat, *Liq. Cryst.*, 2012, **39**, 303–312.

183 C. Lavigueur, E. J. Foster and V. E. Williams, *J. Am. Chem. Soc.*, 2008, **130**, 11791–11800.

184 B. Bai, C. Zhao, H. Wang, X. Ran, D. Wang and M. Li, *Mater. Chem. Phys.*, 2012, **133**, 232–238.

185 R. Kleppinger, C. P. Lillya and C. Yang, *J. Am. Chem. Soc.*, 1997, **119**, 4097–4102.

186 K. Kishikawa, S. Furusawa, T. Yamaki, S. Kohmoto, M. Yamamoto and K. Yamaguchi, *J. Am. Chem. Soc.*, 2002, **124**, 1597–1605.

187 M. D. Miranda, F. Vaca Chávez, T. M. R. Maria, M. E. S. Eusebio, P. J. Sebastião and M. Ramos Silva, *Liq. Cryst.*, 2014, **41**, 1743–1751.

188 J. H. Lee, S. J. Lee and J. Y. Jho, *Phase Transitions*, 2014, **87**, 656–665.

189 E. Beltrán, E. Cavero, J. Barberá, J. L. Serrano, A. Elduque and R. Giménez, *Chem. Eur. J.*, 2009, **15**, 9017–9023.

190 H. K. Singh, S. K. Singh, R. Nandi, M. K. Singh, V. Kumar, R. K. Singh, D. S. S. Rao, S. K. Prasad and B. Singh, *RSC Adv.*, 2015, **5**, 44274–44281.

191 Y. Wu, C. Zhang, Y. Zhang, B. Bai, H. Wang and M. Li, *Liq. Cryst.*, 2014, **41**, 1854–1861.

192 M. Marechal, A. Cuetos, B. Martínez-Haya and M. Dijkstra, *J. Chem. Phys.*, 2011, **134**, 094501.

193 A. Patti, S. Belli, R. van Roij and M. Dijkstra, *Soft Matter*, 2011, **7**, 3533–3545.

194 A. Cuetos and B. Martínez-Haya, *J. Chem. Phys.*, 2008, **129**, 214706.

Molecular dispersity in binary discogen mixtures leads to induced columnar mesophases, an effect dependent on the extent of thickness bidispersity.